Identification of Atlantic water inflow on the north Svalbard shelf during the Holocene

Marion Peral[1,2,3], William E.N. Austin[1,4], Riko Noormets[5]

1. *School of Geography & Sustainable Development, University of St Andrews, St Andrews, KY16 9AL, UK*
2. *EPOC, UMR 5805, CNRS, University of Bordeaux, Pessac, France*
3. *Now: Analytical, Environmental and Geo-Chemistry, Vrije Universiteit Brussel, Pleinlaan 2, Brussels 1050, Belgium.*
4. *Scottish Association for Marine Science, Scottish Marine Institute, Oban, Argyll, PA37 1QA, UK*
5. *Department of Arctic Geology, The University Centre in Svalbard (UNIS), Longyearbyen N-9171, Norway*

Abstract

Nordaustlandet is located in the northeastern part of the Svalbard archipelago, within the northernmost reach of the West Spitsbergen Current. This current transports Atlantic water to the Arctic Ocean along the western and northern Svalbard margins. This region is well-suited for reconstructing the history of changing Atlantic water inflow to the Arctic Ocean. We studied the marine sediment core HH12-04-GC from Rijpfjorden. Benthic foraminiferal assemblages and sedimentological data are combined to reconstruct the paleoenvironment of the fjord from the end of the last local deglaciation to the late Holocene. The local deglaciation, between 11.3 and 10.6 cal. ka BP, was dominated by active glacier calving processes, associated with a strong inflow of Atlantic water. This led to the establishment of glaciomarine conditions. The Holocene was initially characterized by a relatively stable and warm environment associated with a strong contribution of Atlantic water. Glaciomarine influence progressively decreases after 9.7 cal. ka BP and Atlantic water contribution increases. The late Holocene display similar environment to today, with the influence of glaciomarine conditions and limited Atlantic water inflow. These results confirm that Atlantic water inflows made a continuous contribution to northern Nordaustlandet throughout the postglacial period.

Keywords: Paleoenvironment and paleoceanographic reconstructions, Nordaustlandet, Rijpfjorden, benthic foraminifera, sediments

1. Introduction

The Arctic Ocean is one of the most sensitive regions in its response to climate change. The transport of warm and saline water from the Atlantic Ocean through surface and sub-surface currents flowing into the Arctic Ocean has a fundamental role in determining regional

climates. The heat transported to the Arctic region by these currents affects both sea ice extent and, by extension, albedo. As a result of these climate feedbacks and interactions, anthropogenic warming is expected to be accelerated in the Arctic region. The term Arctic amplification is used to explain the special sensitivity of the high latitudes to climate change (Manabe and Stouffer, 1980; Serreze and Francis, 2006; Serreze et al, 2009; Cohen et al., 2014).

The Svalbard archipelago is located in the Arctic, in the northern Barents Sea, between 76° and 81°N (Figure 1). Its connection to the Atlantic Ocean via the Norwegian Sea determines responses and feedbacks to climate change by heat transportation and, as that heat is released to the atmosphere, allows deep water to be generated by convection processes in the Nordic seas (Aagaard and Greisman, 1975). The West Spitsbergen Current (WSC) flows via Fram Strait between Svalbard and Greenland (Figure 1) and acts as the major gateway between the Arctic Ocean and water masses originally deriving from the Atlantic Ocean (Aagaared and Greisman, 1975; Saloranta and Haugan, 2001). Because of its likely sensitivity to changes in the intensity of Atlantic Water inflow over recent geological time, the Svalbard archipelago is ideally located to study the variations of Atlantic water inflows into the Arctic Ocean. While the west and south coasts of Svalbard and the Barents Sea regions have been investigated in previous studies from the last deglaciation to the late Holocene (Polyak and Mikhailov, 1996; Lubinski et al., 1999; Hald and Aspeli, 1997; Hald et al., 1994, 2001, 2004, 2007; Duplessy et al., 2001; Schlichtholz and Goszczko, 2006; Rasmussen et al, 2007; Kubischta et al., 2011; Werner et al., 2011; Jessen et al., 2010; Hormes et al., 2013; Klitgaard-Kristensen et al., 2013; Rigual-Hernández et al., 2017; Nielsen and Rasmussen, 2018; Ivanova et al., 2019; Pawłowska et al., 2020), the north Svalbard margin and its palaeoceanographic evolution since the last deglaciation remains poorly known, mainly due to the lack of complete marine records with good time resolution. Relatively few records on glacial landform, from the last deglaciation are currently available from the northern Svalbard margin (Koç et al., 2002; Ślubowska et al., 2005, Ślubowska-Woldengen et al., 2007, Rasmussen et al., 2014; Chauhan et al., 2016, Fransner et al., 2017; Brice et al., 2020).

Here, we study a sediment core taken from the inner shelf north of Nordaustlandet, adjacent to Rijpfjorden (core HH12-04-GC; Figure 1). Using foraminiferal assemblages, we identify the source(s) of water masses present in the fjord (e. g. Atlantic-, Arctic-origin) in order to reconstruct the oceanographic circulation in the past, which is still poorly documented for this region. This study aims to identify the inflow of Atlantic water into the area north of Nordaustlandet, from the end of the last deglaciation to the late Holocene. Pre-existing

lithological data (Fransner et al., 2017) and distribution of benthic foraminifer are combined to document the interaction between oceanographic and glacial conditions in this fjord, which is subjected to a glaciomarine environment. These results constitute a new marine dataset from the easternmost part of the WSC and are compared to previously published data from the western part of the Svalbard margin.

2. Geographic and oceanographic settings

The Barents Sea is a relatively shallow, continental shelf sea with a mean water depth of 230 m. In the southern part of the Barents Sea, North Atlantic Water (NAW) remains close to the surface and is characterized by salinities higher than 35.0 and temperature from 3.5° to 6.5°C in summer (Locarnini et al., 2018; Zweng et al., 2013). Both temperature and salinity decrease northeastwards. In the southern Barents Sea, NAW occupies most of the water column (Risebrobakken et al., 2011), while in the northern Barents Sea, NAW is mostly found at depths between 120-200 m (Duplessy et al., 2001). During winter, Arctic water, originating from the north and characterized by low salinity (below 34.3) and sea surface temperatures below 0°C, occupies the upper 150 m of the water column (Locarnini et al., 2018; Zweng et al., 2013). During summer, the surface water layer between 5-20 m incorporates a pronounced meltwater signature with very low salinity, below 34 (Helland-Hansen and Nansen, 1909; Otto et al., 1990; Hopkins, 1991; Huthnance et al., 1991).

The NAW flows to the Arctic Ocean via two pathways (Figure 1). First, the eastern branch of the Norwegian-Atlantic Current (NwAC) bifurcates to Fram Strait in the Barents Sea towards the Arctic Ocean via the North Cape Current (NCaC; Figure 1). Second, NAW is guided by the deep-sea topography in the middle of the Nordic Seas to circulate in Fram Strait (Figure 1, Werner et al., 2011). Fram Strait therefore represents the major gateway between the Arctic Ocean and water masses deriving from the Atlantic Ocean. The NAW flows northward in the WSC and is constrained by the Knipovich Ridge (Aagaard and Greisman, 1975; Saloranta and Haugan, 2001). The WSC submerges in Fram Strait at about 78°N to form the Atlantic Layer (Aagaard and Carmack, 1989). The WSC follows the morphology of the seafloor (Rudels, 1987; Pfirman et al., 1994) and splits into three currents to the north of Svalbard at around 79.9°N (Figure 1). The Yermak Branch (YB) flows to the northwest into the Arctic Ocean (Manley, 1995). The Return Atlantic Current (RAC) flows to the Greenland Sea (Schlichtiolz and Goszczko, 2012), while the Svalbard Branch (SB) follows the north and

105 east coast of the Svalbard archipelago, supplying the major portion of the NAW into the Arctic
106 Ocean (Figure 1; Aagaard et al., 1985; Manley, 1995; Rudels et al 1999).
107 Rijpfjorden is one of the two major fjords of Nordaustlandet. This fjord has a south-
108 north orientation and is open to the Arctic Ocean in the north (Figure 1). Rijpfjorden is located
109 in the northernmost part of the WSC. The NAW, transported in the SB of the WSC, flows along
110 the continental slope, as the Atlantic Water Boundary Current (AWBC), and resides at the
111 upper continental slope and occasionally extends onto the shelf, with temperatures reaching
112 3°C and salinity up to 35 (Hop et al., 2019). The Winter Cooled Water (WCW) is the dominant
113 water mass in the fjord, but its contribution declines toward the open shelf. By contrast, Arctic
114 Intermediate Water dominates the shelf-edge and declines toward the continental slope and
115 shelf (Hop et al., 2019). Polar Surface Water (temperatures below 0°C and salinity below 33)
116 is generally restricted to the upper 100 m of the water column and results in the stratification
117 of the water column. This present-day configuration places the Arctic Polar front on the
118 continental slope and sea ice cover within the fjord varies considerably between years (Hop et
119 al., 2019).
120 Glacial and post-glacial sediments are deposited on top of the Late Precambrian
121 bedrock (Elverhøi and Lauritzen, 1984). These sediments are influenced by mass-flow
122 processes, contour currents and sediment deposition from sea ice and icebergs (Chauhan et al.,
123 2016 in Barents Sea region; Fransner et al., 2017 more specifically in Rijpfjorden). Nearly 80%
124 of Nordaustlandet is covered by glaciers at present (Dowdeswell et al., 2010). Two ice caps,
125 Austfonna and Vestfonna, cover a major part of the island to the east and west, respectively
126 (Hagen et al., 1993). The glacial activity of the Late Quaternary has largely shaped the modern
127 landscape, with additional modification by Holocene coastal, fluvial and terrestrial (slope)
128 processes (Fransner et al., 2017). Today, Rijpfjorden is typically covered with sea ice for
129 almost 9 months a year (Ambrose et al., 2006; Leu et al., 2011). With break-up typically
130 occurring between mid-July and mid-August, however, even after break-up, the fjord has very
131 few ice-free days (Leu et al. 2011).
132
133 **3. Paleoenvironmental changes in Svalbard Archipelago from the last deglaciation**
134
135 The last deglaciation is characterised by evidence for the disintegration of the Svalbard-
136 Barents Sea Ice Sheet (SBSIS), the break-up of which appears to have been gradual over time
137 around the Svalbard Archipelago. In Rijpfjorden, the initiation of local-ice melting is dated at
138 12.8 +/- 1.5 ka BP (Hormes et al., 2011). Later deglaciation ages are suggested in the eastern

part of the Svalbard archipelago, between 11.4 and 9.8 ka BP. In marine records from the west and south coast of Spitsbergen, indicators of regional deglaciation largely disappear from sediment deposited after 10.1 ka BP (Jessen et al., 2010; Hormes et al., 2013; Rigual-Hernández et al., 2017; Nielsen and Rasmussen, 2018). This deglaciation allowed the establishment of the present-day ocean circulation. The Bølling-Allerød (14.5 ka) is marked by a strong inflow of Atlantic waters, with a subsequent decrease of Atlantic water influence on the north Svalbard shelf and an increase of ice sheet extent during the Younger Dryas between 12.8 to 11.68 ka (Ślubowska et al., 2005, Ślubowska-Woldengen et al., 2007). The Arctic front, defined as the transition between the dominating Atlantic (south) and Arctic (north) waters, followed the western margin of the Barents Sea until 11 ka BP and then migrated eastwards into the southwestern Barents Sea (Risebrobakken and Berben, 2018). Along the west coast of Svalbard, synchronous oceanographic changes in flow of Atlantic water are recorded through the last deglaciation to late Holocene (Ślubowska et al., 2005, Ślubowska-Woldengen et al., 2007; Rasmussen et al., 2014). Along the eastern and to the Eurasian margin, the strong stratification of the water column indicates stronger Atlantic Water influence in bottom water (Ivanova et al., 2019), accompanied by increased heat advection through the Norwegian Current (Risebrobakken et al., 2011). During the deglaciation, the seawater temperature was the most important forcing factor of the Svalbard-Barents Sea Ice Sheet (Rasmussen et al., 2021). Until 9.6 ka BP, the water column from the Barents Sea to the north of Svalbard was stratified, with cold Arctic water and meltwater above 100 m depth, while below, warm Atlantic water was present (Lubiski et al., 2001; Sarnthein et al., 2003; Rasmussen et al., 2007, 2012, 2014; Ślubowska-Woldengen et al., 2007; Aagaard-Sørensen et al., 2010; Chirstyakova et al., 2010; Risebrobakken et al., 2010; Barben et al., 2014; Ivanova et al., 2019). After 9.6 ka BP, the influence of cold surface Arctic water and meltwater decreases, and sea surface temperatures reached their maximum between 9 and 6 ka BP. This thermal optimum was influenced by the increasing dominance of warm Atlantic water, which dominated the full water column and a change in northwest Barents Sea Arctic front (Risebrobakken et al., 2011; Eldevik et al., 2014; Rasmussen et al., 2014; Sternal et al., 2014; Risebrobakken and Berben, 2018; Ivanova et al., 2019). The presence of Mytilus edulis is observed on a large part of the coasts of Svalbard from 9.4 cal. ka BP, indicative of a climatic optimum, and disappeared during the Holocene, suggesting a limited influence of the warm waters of the Atlantic north of the Svalbard archipelago (Salvigsen et al., 1992; Salvigsen, 2002). From 5 to 2 ka BP, the bottom and surface water temperatures decrease, and the last 2000 years are marked by strong unstable conditions with slightly increasing of subsurface temperatures (Rasmussen et al.,

2014). From the last 3 – 4 ka, in the Kvitøya Trough, cool surface water and enhanced of seasonal sea-ice cover is recorded (Müller et al., 2012; de Vernal et al. 2013; Werner et al., 2013; Eldevik et al., 2014).

4. Material and Methods

A 183 cm long gravity core HH12-04-GC (80°31.57N, 21°40.16E) was recovered from the inner shelf of Rijpfjorden in the north of Nordaustlandet, at 150 m water depth (Figure 1), during the 2012 cruise by University Centre of Svalbard (UNIS) on board the R/V *Helmer Hanssen*. Sediment sub-samples were taken every 4 centimetres and were desiccated using a freeze dryer and dry sediment weights obtained. Approximately 10 grams of sediment were put back into suspension and agitated with deionized water and washed over three different mesh sizes (>2mm; <2mm to >125µm; and <125µm to >63µm). The residues of sediment and distilled water were dried at 40˚C for 48 hours and dry residues were weighted.

Four levels were selected for radiocarbon dating, requiring 4-5 mg carbonate for standard AMS ^{14}C analysis, between 8-9 cm, 76-77 cm, 134-135 cm and 175-176 cm. Monospecific samples of the benthic species *Nonionellina labradorica* were picked from the fraction < 2 mm to > 125 µm. Unfortunately, due to the general scarceness of dateable material within some sub-samples, additional 1 cm sub-samples were combined between the adjacent stratigraphic levels between 74 to 80 cm, 132 to 138 cm and 172 to 179 cm. The sample from 8-9 cm was dated from three large bivalve valves from the fraction >2mm (Table 1). The analyses were performed at the CHRONO Centre, Queens University Belfast for ^{14}C dating. The AMS ^{14}C dates were converted into calibrated ages using the calibration program CALIB 8.2 (Stuiver et al., 2021) with the application of Marine20, according to Heaton et al., (2020). A modern-day reservoir age (550 years) and local reservoir (ΔR) age correction (71 +/- 21 years) was applied throughout (Mangerud et al., 2006). The ages are reported as calibrated years before present (BP).

The washed and dried >125µm fraction was used to pick and count benthic foraminifera because the fraction >63 to <125 µm was relatively poor in foraminifera. The foraminifera have well preserved tests throughout. According to Fatela and Taborda (2002), the confidence limits of benthic foraminiferal counts in assemblages are dependent on the study environment and the number of species present. The number of species identified depends on the count number, which provides a guide to the minimum number of specimens that should be counted

(details for five samples are given in supplementary material Figure SM1). In our samples, a mean minimum value of 161 foraminifera picked yielded a significant result in the assemblages (Figure S1). Where possible, a minimum of 200 foraminifera were therefore picked in order to yield a statistically significant result in the assemblage composition of each sample. Planktic foraminifera were not identified to species-level due to the generally very low abundances in these samples; a count of total planktic foraminifera was recorded. The concentration of foraminifera was calculated as the number of specimens per gram dry bulk sediment, using C2 software. A total of 45 samples were counted, yielding a total of 32 different species (data in supplementary material Table SM2). Fifteen were defined as indicator species, corresponding to species that serve as a measure of environmental conditions and represent at least 1% of the assemblage. These indicator species are illustrated in Plates 1 and 2. Taxonomic identification followed the World Foraminifera Database (Hayward et al., 2021) and is detailed in Table 2, with the ecological preference of each indicator species recorded.

The IRD content was defined by detrital grains in the fraction > 2 mm. Individual lithic fragments were counted for each sample and IRD were calculated as the number of mineral grains in the > 2 mm grain size fraction per gram dry weight sediment.

5. Results

5.1. Chronological results

The conventional and calibrated age data (calibrated years BP, where present = 1950) are shown in Table 1. The radiocarbon ages highlight that the core HH12-04-GC records the Holocene according to Walker et al. (2009). The calibrated ages suggest very high sediment accumulation rates in the early Holocene, with a potential hiatus or very low sediment accumulation rates above 70-76 cm.

The dated level at 134-138 cm (UBA-25666) yielded an older age than expected for this sample based on stratigraphy. This age-reversal may be due to a reworking of older material of sediment and foraminifera at this core depth. In Rijpfjorden, the rapid changes in lithology and lack of retreat moraines suggests a rapid deglaciation, possibly through lift-off of the glacier from its bed (Fransner et al., 2017). This may explain the reverse age in the lower part of the core. Due to the potential error (age reversal) with the date UBA-25666, together with large uncertainties in marine radiocarbon reservoir ages in the Arctic, the results are

interpreted as a function of large and informally defined intervals of time (end of deglaciation and Holocene), and not considered to be reliable for the attribution of precise (calibrated) ages.

5.2. Lithological observations

Individual lithic fragments in the fraction > 2mm have been counted and are reported as normalized concentrations to a standard weight equivalent of each sample (Figure 2). The higher concentrations are found from the bottom of the core to 142 cm. The concentrations are relatively low (< 0.02 grains/gram) throughout the rest of core, with the exception of a noticeable peak at 79 cm, with up to 0.13 grains/gram (Figure 2). The clast composition, constant throughout the core, shows the presence of quartz and black minerals, most likely to be plagioclase or biotite (Figure 2), suggesting a granitic origin for the rock fragments. Similar colour and composition throughout suggest a similar rock source for these clasts. The south of Nordaustlandet is dominated by Caledonian basement rocks and the north by Pre-Devonian basement rocks (Johansson et al., 2001). These units are constituted of granite containing quartz, plagioclase, pink K-feldspar, muscovite and biotite; they are dated to the Silurian-Devonian by Krasil'Ščikov et al., (1964). To the west, volcanic rocks, including granites, have been identified as part of the Murchisonfjorden supergroup (Johansson et al., 2001). The composition of the clasts observed in the core suggests their local origin. Their subangular shapes suggest an iceberg debris origin (IRD).

5.3. Foraminiferal analyses

Fifteen species have been defined as indicator species (list in Figure 3). All of them yield a concentration up to 1% of the total assemblage. The variations in the abundance of all these indicator species allow the determination of four foraminiferal assemblage zones, which are summarised in the faunal diagram (Figure 3).

- **Assemblage zone 4**: *Elphidium clavatum*, *Cassidulina reniforme* and *Nonionellina labradorica* zone (138cm to bottom)

Assemblage zone 4 is defined by a high percentage of *Elphidium clavatum* (Plate 1, image b and c), *Cassidulina reniforme* (Plate 1, image a) and *Nonionellina labradorica* (Plate 2, image c, d and e), representing around 80 % of the total assemblages. Toward the top of the unit, the abundance of *N. labradorica* (from 17 to 9%), *Stainforthia fusiformis* (Plate 2, images h and i;, from 4 to 0.5%), *Cibicides lobatulus* (Plate 2, image a and b; from 5 to 0%) and *Stainforthia*

loeblichi (Plate 2, image j; from 5 to 0%) decrease. Despite very low percentages, the presence of *Elphidium albiumbilicatum* (Plate 1, image e) and *Islandiella norcrossi* (Plate 1, image g) are recorded at the bottom of the core, respectively at around 0.7% and 1.8%.

- **Assemblage zone 3**: *Elphidium clavatum*, *Cassidulina reniforme* zone (78cm to 138cm)

Assemblage zone 3 is dominated by *E. clavatum* and *C. reniforme* with mean relative abundances of 23 % and 45 %, respectively. *Elphidium asklundi* (Plate 1, image d) abundance increase toward the top of the zone from 2.7% to 5.7%. This zone marks a transition to a generally very low abundance of other species, except at a core depth of 118-119 cm, where a peak of *Islandiella helenae* (Plate 1, image f)*, I. norcrossi, Cribrostomoides crassimargo* (Plate 2, image k) and broken specimens occurs, respectively at 34.5%, 29%, 16.4% and 5.5%. At the top of the zone, *N. labradorica* appears with a mean abundance of 6%.

- **Assemblage zone 2**: *Cibicides lobatulus*, *Melonis barleeanum* and *Buccella tenerrima* (18cm to 78cm)

Assemblage zone 2 shows the dominance of *C. lobatulus*, *Melonis barleeanus* (Plate 1, image h) and *Buccella tenerrima* (Plate 2, image f). Their abundance increases from 70 cm (respectively up to 41%, 14% and 10%) followed by a decrease up core after 40cm (respectively to 18%, 5% and 2%). Broken specimens present a synchronous increase alongside *C. lobatulus*, with an increase in the abundance from 4% to 13.5% at 56-57cm and a progressive decrease to 4%. The abundance of *M. barleeanum* is constant throughout the zone, around 8.4%. *N. labradorica* and *S. loeblichi* decrease rapidly from the bottom of this zone, respectively from 47.5% to 1% and from 4.5 to 0%. *I. norcrossi* decreases gradually from 21 to 2% toward the top of Assemblage 2. At the opposite, *E. albiumbilicatum, E. clavatum* and *C. reniforme* increase from 1.8% to 13.7%, 1% to 10% and 2.4% to 25.5%, respectively. The presence of *I. helenae* (4%)*, E. asklundi* (1.7%) and planktic foraminifera (0.4%; Plate2, image g) is noted in low abundance throughout the Assemblage 2.

- **Assemblage zone 1**: *Cassidulina reniforme* and *Islandiella helenae* zone (0 to 18cm)

Assemblage zone 1 consists of a high percentage of *C. reniforme* decreasing from 42% to 26.8%, and *I. helenae* with a maximum of 18% at 4-5cm. *M. barleeanum* (from 11% to 16%) also increase toward the top of the assemblage zone. *E. clavatum* (from 7% to 11%), *I. norcrossi* (around 6%) and *B. tenerrima* (from 1% to 6%) are recorded. The abundance of *C. lobatulus* and *E. albiumbilicatum* decreases toward the top of the core from 10% to 6.7% and 15 to 8.5%, respectively. Broken specimens (2.5%), *E. asklundi* (2%) and planktic foraminifera (0.6%) are also found at the top of the core in low abundance.

6. Interpretations

Lithological summary

Here, we summarize the lithological interpretations of the core, and present images of the clast recorded in the size fraction >2mm. The sedimentological records are based on Fransner et al. (2017); these data were obtained by combining Munsell colour codes and physical properties: density, magnetic susceptibility, shear strength and grain size using a laser particle size analyser. The physical properties corresponding to the first 19 cm of the core are not available (Fransner et al., 2017). In Figure 2, the lithological log and grain size curve are plotted with the images of the outsized clasts from different levels and the ^{14}C dates. Three lithofacies were identified by Fransner et al. (2017):

Lithofacies 3: from the base of core to 150 cm is characterized by a sandy sediment with mud lenses and a decrease of grain size from diamicton at its lower part to coarse sand (Figure 2). Subangular clasts are identified up to 20 mm-long (Figure 2). The diamicton could be subglacial deformation till (e.g., Alley et al., 1987; Hogan et al., 2010), dropstone diamicton, or possibly basal meltout-till (Harland et al., 1966; Dreimanis, 1976). The presence of sandy mud lenses may represent plume deposits from glacial meltwater discharge (Powell, 1984) as interpretated in Fransner et al. (2017). The evidence of a rapid fining-upwards diamicton and transition to silt sediments is the likely product of iceberg delivery of heterogeneous debris (Dowdeswell et al, 2000).

- **Lithofacies 2**: between 66 and 149 cm, the core is dominated by silty mud, rich in outsized clasts (<20 mm in diameter). The 75 cm level is marked by the top of the silty mud rich in outsized subangular clasts (Figure 2). This high concentration of outsized large clasts in a fined-grain mud indicates a glaciomarine depositional environment under influence of IRD deposition (Fransner et al., 2017).
- **Lithofacies 1**: from 66 cm to the top of the core, a massive silty mud is recorded with a high ratio of outsized clasts of around 10-20% (Figure 2). The last 15 cm records the presence of shells and shell fragments, and sub-angular clasts, which are smaller than those observed in the rest of the core (Figure 2). This lithofacies is interpreted as marine mud (Fransner et al., 2017).

Foraminiferal summary

Here, we summarized the interpretations of the paleoenvironmental changes in response to foraminiferal distribution, withing the four assemblage zones defined above.

The assemblage zone 4 in the foraminiferal diagram (Figure 3) is dominated by *C. reniforme* and *E. clavatum,* which are typical of glaciomarine conditions in Svalbard fjords (cold water). This dominance suggests that the core site was in a distal position from glacier fronts, with potentially some sea ice cover (Elverhøi et al., 1983; Hald & Vorren, 1987; Hald et al., 1994; Hald & Korsun, 1997). A diminution of *S. loeblichi* abundance is often interpreted by a decrease in organic matter influx and/or an increase of the salinities (Feyling-Hanssen, 1964; Alve, 1994). The decrease in abundance of the opportunist *N. labradorica* may indicate a progressive decrease of Atlantic water inflow and suggests that the Arctic front moved away from the core site (Corliss, 1991; Steinsund, 1994). These changes were accompanied by reduced numbers of *C. lobatulus*, often found in sandy or coarser sediments, often correlated with increasing bottom current strength (Murray, 1991, 2006; Steinsund et al., 1994).

The assemblage zone 3 (Figure 3) is dominated by *E. clavatum* and *C. reniforme*. Corelated with the presence in low abundance of *E. asklundi,* it indicates glaciomarine conditions, close to glaciers and ice caps (Austin, 1991; Polyak and Solheim, 1994; Hald et al., 1994; Hald and Korsun, 1997). The significant decrease toward the zone 4 in the abundance of the *N. labradorica* and the low abundance of *C. crassimargo* indicate a more stable environment. *C. crassimargo* reflects a relatively long ice-free summer period (Lloyd, 2006), also suggesting an increase of cold meltwater input. The presence of *I. helenae* and *I. norcrossi,* with the simultaneous peak of *C. crassimargo,* at the core depth 122 cm, is interpretated as indicative of relatively cold water, with stable bottom salinity and hight productivity (Mudie et al., 1984; Steinsund et al., 1994; Korsun and Hald, 1998; Rytter et al., 2002; Cage et al., 2021). These observations point to a northward retreat of the Arctic Costal Front at this time.

The abundance of the dominant species decreases in the first centimetres (top) of the zone accompanied by an increase of *M. barleeanus, N. labradorica* and *I. norcrossi*, consistent with the presence of nutrient rich Atlantic Water. These changes in foraminifera assemblages show an increase in the influence of Atlantic water and suggest a southward shift of the arctic front to our main site. However, the increasing proportions of *I. helenae* suggests stable salinity condition (Hald and Korsun, 1997).

The assemblage zone 2 is characterized by a rapid decrease of *E. clavatum* and *C. reniforme* abundances, indicating an interruption of glaciomarine conditions. At the bottom of the zone, *N. labradorica* is present in relative high percentages and decreases rapidly across the zone, suggesting that the Arctic front retreated northward from the core site. The dominant *C. lobatulus* is associated to strong current regimes (Korsun and Polyak, 1989; Steinsund et al., 1994) and is strongly correlated with the high percentage of broken (random) specimens. The *B. tenerrima* abundance increase is also correlated to the changes observed in *C. lobatulus* abundance. This species is related to high surface ocean seasonal productivity and to sea ice cover (Mudie et al., 1984; Polyak and Solheim, 1994). The presence of *M. barleeanus* indicates a change from abundant fresh organic matter supply to a more degraded/recalcitrant organic matter supply at the sea floor (Caralp, 1989; Korsun and Polyak, 1989). Coupling the increase of *E. albiumbilicatum* with the presence of *I. norcrossi* (both sub-artic) and the decrease of *I. helenae* (arctic) suggests the progressive input of Atlantic water and decrease of sea-ice at the core site (Cage et al., 2021).

The assemblage Zone 1 (Figure 3) shows a dominance of *C. reniforme*. Despite the increase of *E. clavatum*, *C. reniforme* dominates the assemblage by up to 30%, highlighting the presence of sea ice cover (Hald et al., 1994; Elverhøi et al., 1983). The low abundance of arctic (*I. helenae* and *B. tenerrima*) and sub-arctic (*C. lobatulus*, *I. norcrossi and E. albiumbilicatum*) species is interpreted as a response to the presence of the sea ice cover in relatively unstable conditions (Ślubowska-Woldengen et al., 2007) and may highlight a complexity in bottom water structure with influence of cold meltwater, Atlantic and Arctic waters.

7. Discussion

7.1. Chronology of the core

The bottom of the core is characterized by diamicton lithofacies (Lithofacies 3, Figures 3&5), which suggests a glacial influence with subglacial deformation and plume deposits from glacial meltwater discharge (Fransner et al., 2017). Between 171 and 179 cm, the median age is 10,557 cal. yrs BP, corresponding to the beginning of the Holocene (Walker et al., 2009); a median age of 11,318 cal. yrs BP at 134-138 cm suggests an age-reversal. However, the presence of *S. fusiformis* at the bottom of core (Figures 3 & 4), is often interpreted as an

indicator of increase productivity/organic matter influx with lowered salinities during the Younger Dryas (Feyling-Hanssen, 1964; Alve, 1994). The local deglaciation may result in the transition to a highly productive (primary productivity) marine environment, in which *S. fusiformis* would typically be found. Its presence, combined with ^{14}C dates and lithological data (see section 7.2) suggests a record of the end of last local deglaciation of the shelf, which was initiated by local-ice melting at 12.8 +/- 1.5 cal. ka BP in the fjord (Hormes et al., 2011). Additionally, age reversal is not uncommon during the deglaciation, especially in the vicinity of a large ice cap with large and dynamic ice streams and potential to calve large icebergs. Both foraminiferal and lithological data suggest deglaciation processes associated to calving at the core site, as it is discussed in the next section.

Both lithofacies 1 and 2 are characterised by homogenous sedimentology with silty mud, which constitute the dominant lithofacies types of the core (Fransner et al., 2017). This unite is radiocarbon dated to the Holocene. Furthermore, similar sedimentological lithofacies are observed from the central and northern Barents Sea (Elverhøi and Solheim, 1983) and in the Kvitøya Trough (Hogan et al., 2010) and date from the Holocene. The uppermost ~10 cm of the core dates to 194 cal. yrs BP. It should be noted the possibility that cold water molluscs may produce somewhat older marine reservoir values compared to other species due to the inclusion of old carbon or vital effect as suggested in Forman and Polyak (1997) and Lo Guidice Cappelli and Austin (2019).

7.2. Paleoenvironmental changes during the end of the last local deglaciation

The sedimentological data (Figures 3 & 4) show, at the bottom of the core, evidence of a rapid fining-upwards diamicton and transition to silt sediments, which is the likely product of iceberg delivery of heterogeneous debris (Dowdeswell et al, 2000). This diamicton deposit is embedded in sandy mud, suggesting that it represents plume deposits from glacial meltwater discharge (Powell, 1984). The lack of retreat moraines at the core site, suggests rapid deglaciation, possibly linked to a surge activity (Fransner et al., 2017). The time of the regional glacier ice break up is synchronous with IRD deposits in marine sediments (Koç et al., 2002). The increase of IRD concentration is therefore thought to be due to the amplification of calving processes, driven largely by warming seawater temperatures as the intensification of Atlantic water inflow into the Arctic Ocean. The dominance of angular > 2mm clasts (Figures 3) at the bottom of the core suggests a glaciomarine diamicton origin, which therefore reflects major and rapid retreat of the glacier front. The dominance of glaciomarine species (Figures 4 & 5)

441 suggests the influence of glacial meltwater discharge. The presence of *N. labradorica* is
442 associated with glacier distal habitats (Korsun and Hald, 1998) and enhanced productivity
443 (Steinsund, 1994). In the Svalbard region, its abundance also reflects the approaching Arctic
444 Coastal Front, which splits Atlantic (i.e., the Svalbard Branch) and Arctic waters. Our benthic
445 foraminifera relative abundance data therefore suggests a transition from unstable bottom
446 conditions under the influence of the Arctic Coastal Front to a stable environment and a rapid
447 retreat of the glacier (i.e. proximal to distal transition) at the core site. Despite the age reversal
448 at the bottom of our core, the inner shelf adjacent to Rijpfjorden was glacier ice-free between
449 11.3 and 10.6 cal. ka BP, which is in agreement with the previous study as the deglaciation was
450 complete by 10.6 cal. ka BP in the inner Rijpfjorden and 11.0 cal. ka BP in central Duvefjorden
451 (Fransner et al., 2017).
452 Around the Svalbard margins, since the last deglaciation, the intrusion of Atlantic water
453 is generally linked to the retreat of glaciers, as this subsurface inflow melted tidewater glaciers
454 (Hormes et al., 2013; Jessen et al., 2010; Klitgaard Kristensen et al., 2013; Skirbekk et al.,
455 2010; Ślubowska et al., 2005, 2007). The presence of the Arctic front and the glaciomarine
456 conditions suggest an enhancement of the Atlantic water flow which destabilized the ice and
457 promoted the calving process (Figure 5 - A). Similar distributions of *N. labradorica* during the
458 deglaciation (Figure 4) are recorded on the northern Svalbard continental slope (Koç et al.,
459 2002; Ślubowska et al., 2005; Rasmussen et al., 2014) and from western Spitsbergen
460 (Ślubowska-Woldengen et al., 2007).
461
462 **7.3. The Holocene paleoenvironments**
463
464 There is a high degree of similarity between our foraminiferal assemblages and
465 assemblages from the west and north coast of Svalbard in the Holocene (Figure 4; Ślubowska
466 et al., 2005; Ślubowska-Woldengen et al., 2007, Skirbekk et al., 2010; Rasmussen et al., 2012).
467 However, some faunal differences are observed (e.g. absence of *Cassidulina neoteretis*, in our
468 data set, identified as Atlantic water indicators, abundance of *C. reniforme* as explained below),
469 partly expected because of the poor preservation state, most likely associated with corrosive
470 and under-saturated water masses, and partly because of the influence of diverse local
471 environmental factors. The less favourable conditions are also likely to have been caused by
472 the influence of relatively strong currents and occasional freshwater inflow from glaciers under
473 the local glaciomarine conditions.

The Holocene records in this study can be divided into three parts: before and after ~9.7 cal. ka BP and the last ~200 years cal. yrs BP (Figure 4). First, from the end of the last local deglaciation to ~9.7 cal. ka BP, glacimarine conditions dominate (Assemblage Zone 2 - Figure 3; and Lithofacies 2 - Figure 2). Both sedimentology and faunal assemblages suggest stable bottom water condition. The presence of *I. helenae*, *S. loeblichi* and other glaciomarine species suggest that the environment was likely to have been influenced by distal glacier and potentially sea ice cover to open ocean conditions (Figures 4&5); the presence of lower concentrations of outsized clasts than during the deglaciation support this interpretation (Figures 3&5). The very low abundance of cold-tolerant species and the presence of *I. norcrossi* suggests a transition to warmer and more saline conditions and the first part of Holocene is therefore defined by a warmer environment under glaciomarine conditions with potentially seasonal sea-ice cover, pointing to an enhanced influx of Atlantic Water (Figure 5-B). Despite the low abundances of *N. labradorica*, the Arctic front moves northward as Atlantic water and meltwater begin to dominate at this time. At the depth of 122 cm, the environment was perturbed by an increase of high salinity water, high productivity and open ocean indicators, potentially due to local effects and/or the stronger incursion of Atlantic water.

Reconstructed sea surface temperatures show warmer temperatures than today by between 2 and 5ºC along a transect between Norway and the west Svalbard shelf during the Holocene climate optimum (Calvo et al., 2002; Birks and Koç, 2002 and Sarnthein et al., 2003). However, on the west and north Svalbard shelf, the assemblages of planktic foraminifera are dominated by cold species, that may be explained by stratification of the water column with cold Arctic water and meltwater above 100 m depth and warm Atlantic water below (Hald et al., 2004 and Ślubowska et al., 2005, Rasmussen et al., 2014). In the Barents Sea, the early Holocene was marked by a high Atlantic water inflow (e.g., Bauch et al., 2001; Carbonara et al., 2016; Groot et al., 2014; Müller and Stein, 2014; Rigual-Hernández et al., 2017; Risebrobakken et al., 2011; Telesiński et al., 2015; Werner et al., 2013, 2016). This increasing inflow is observed by a bottom warming trend on the west and northern part of the Svalbard Archipelago (e.g., Hald et al., 2004; Rasmussen et al., 2012, 2014; Sarnthein et al., 2003; Skirbekk et al., 2010; Ślubowska et al., 2005; Klitgaard-Kristensen et al., 2013; Rigual-Hernández et al., 2017; Nielsen and Rasmussen, 2018; Ivanova et al., 2019; Ivanova et al., 2019; Pawłowska et al., 2020; Brice et al., 2020).

The second part of Holocene, after ~9.7 cal. ka BP to ~200 years cal. yrs BP, is marked by a decrease of glaciomarine conditions and significant increase of strong bottom current and

high productivity indicators (Figures 4&5 – respectively *C. lobatulus* and *B. tenerrima* & *M. braleeanus*). The sedimentological data also suggest a change from glaciomarine to marine muds (Figures 3&5). The low sedimentation rate of our top 70 cm (based on our ^{14}C dates) is strongly correlated to the high abundance of *C. lobatulus* and broken specimens (Figures 4&5) and to the decrease of clay and increase of silt and sand in the 1 mm fraction (Figure 2 – grain size Dx, from Fransner et al., 2017). These data provide clear evidence that this low sedimentation rate was driven by increased bottom current velocity at the core site. Interestingly, grain size data (sorted silt) from the shelf edge/upper slope environment north of Nordaustlandet also suggests increased current velocity and resulting decrease in sedimentation rate (Chauhan et al., 2016). The faunal assemblages indicate that the relatively high energy environment at the sea floor decreases and a reduction in the influence of the Arctic front and glaciomarine conditions. The enhancement in current velocity and productivity and presence of "warmer – saline" water species, may point to an enhancement of Atlantic water inflow to the core site. After 9.7 cal. ka BP, similar assemblages are observed around the Svalbard margins, marked by the presence of indicator species such as *Buccella* spp. and *M. barleeanum* (Figure 4). As the dominance of cold surface Arctic (and meltwater) water decreases, and sea surface temperatures reached their maximum between 9 and 6 ka BP (Rasmussen et al., 2014), warm Atlantic waters begin to dominate the full water column (Rasmussen et al., 2014; Risebrobakken and Berben, 2018). However, this time interval is also marked by the abundance (~20%) of arctic species (Figure 3), which suggests the continued influence of Arctic water and sea ice cover (Figure 5-C). Indeed, seasonal sea ice also persisted through the Holocene in the north and east part of the Svalbard archipelago (Pienkowski et al., 2021). The presence of low abundances of *N. labradorica* also suggest the proximity of the Artic front (Figures 4&5-C). These observations point to a regionally cold climate, influenced by warm Atlantic water on the north Svalbard shelf.

The last ~200 years cal. yrs BP is marked by massive marine muds characteristic to low energy depositional environments (Fransner et al., 2017: suspension setting; Elverhøi and Solheim, 1983), supported by decreases of *C. lobatulus* and weaker bottom current velocity. The presence of glaciomarine species increases at this time, accompanied by an increase of sea ice cover indicators (Figures 4&5). However, rare and smaller outsized clasts indicate little IRD production (Figure 2; Plassen et al., 2004; Fransner et al., 2017) and support our interpretation of glaciomarine conditions (Figure 5-D). Several previous studies have recorded abundant glaciomarine species through this time period (Figure 4; Ślubowska et al., 2005;

Ślubowska-Woldengen et al., 2007; Skirbekk et al., 2010; Rasmussen et al., 2012). The presence of *I. helenae* and *B. tenerrima* suggest cool bottom water with a low and stable salinity. However, the present of Atlantic water indicator species are noticeable (Figure 3). Our data are in good agreement with the present-day conditions at the core site, which are dominated by Polar Surface Water, characterized by low salinity and probably due to sea ice melt and glacier run-off into the fjord (Hop et al., 2019). Bottom waters share an influence from Arctic Intermediate Water and the Winter Current Water, resulting in sea ice formation and associated convection during intense cooling (Cottier et al., 2005; Hop et al., 2019). The Arctic front is located on the continental slope (north of the core site), despite a relatively small contribution of Atlantic Water at the seabed on the inner shelf (Hop et al., 2019). These present-day conditions show an important influence from glaciomarine conditions at our core site, with variable inter-annual presence of sea ice cover (Hop et al., 2019).

Conclusion

This study documents changes in bottom water conditions in the inner shelf north of Nordaustlandet (off Rijpfjorden) over the late glacial and Holocene. The geographical location of the core site is today under the influence of glaciomarine, and marine processes and this influence is considered likely to have changed with time. Based on foraminiferal analyses and sedimentological data these paleoenvironmental changes were reconstructed. The end of the last deglaciation is marked by diamictic deposits which are associated with active glacier calving process. The inflow and presence of Atlantic water on the north Svalbard shelf led to the establishment of glaciomarine conditions and the northward retreat of the Artic front. The early Holocene is therefore marked by a strong contribution of Atlantic water, yet the study site remained under glaciomarine conditions and was characterized by seasonal sea ice cover. After 9.7 cal. ka BP, Rijpfjorden recorded a decrease of glaciomarine conditions and a significant increase of bottom current velocity and high productivity indicators, suggesting a strengthening inflow of Atlantic water. However, the presence of Artic water species is noticeable during this period, suggesting the proximity of the Arctic front. Over the last 200 years, a relatively similar configuration to present-day conditions at the core site highlights the continued influence of glacimarine environments and a weak contribution of Atlantic water. Within the limits of the large dating uncertainties, similar oceanographic changes are observed in several published studies around Svalbard; all pointing to the presence of sub-arctic faunal components after regional deglaciation had occurred. Our results therefore confirm that

574 Atlantic water inflow made a continuous contribution to the bottom water of Nordaustlandet,
575 flowing from the west to the north Svalbard shelf, throughout the Holocene.
576
577
578 **Reference**

579 Aagaard, K., & Greisman, P. (1975). Toward new mass and heat budgets for the Arctic
580 Ocean. *Journal of Geophysical Research*, *80*(27), 3821-3827.
581 Aagaard, K., Swift, J. H., & Carmack, E. C. (1985). Thermohaline circulation in the Arctic
582 Mediterranean seas. *Journal of Geophysical Research: Oceans*, *90*(C3), 4833-4846.
583 Aagaard, K., & Carmack, E. C. (1989). The role of sea ice and other fresh water in the Arctic
584 circulation. *Journal of Geophysical Research: Oceans*, *94*(C10), 14485-14498.
585 Aagaard-Sørensen, S., Husum, K., Hald, M., Knies, J. (2010). Paleoceanographic development
586 in the SW Barents Sea during the Late Weichselian–Early Holocene transition. *Quaternary*
587 *Science Reviews* 29, 1–15.
588 Alley, R. B., Blankenship, D. D., Rooney, S. T., & Bentley, C. R. (1987). Till beneath ice
589 stream. *Journal of Geophysical Research: Solid Earth*, *92*(B9), 8931-8940.
590 Alve, E. (1994). Opportunistic features of the foraminifer Stainforthia fusiformis (Williamson):
591 evidence from Frierfjord, Norway. *Journal of Micropalaeontology*, *13*(1), 24-24.
592 Alve, E., & Murray, J. W. (1999). Marginal marine environments of the Skagerrak and
593 Kattegat: a baseline study of living (stained) benthic foraminiferal
594 ecology. *Palaeogeography, Palaeoclimatology, Palaeoecology*, *146*(1-4), 171-193.
595 Ambrose, WGJ, Carroll, ML, Greenacre, M, Thorrold, SR and McMahon, KW (2006). Variat
596 ion in *Serripes groenlandicus* (Bivalvia) growth in a Norwegian high-Arctic fjord:
597 evidence for local- and large-scale climatic forcing. *Global Change Biol.*, 12(9), 1595–
598 1607 (doi: 10.1111/j.1365-2486.2006.01181.x)
599 Austin W. 1991. Late quaternary benthonic foraminferal stratigraphy of the western U. K.
600 continental shelf (Doctoral dissertation, University College of North Wales).
601 Berben, S.M.P., Husum, K., Cabedo-Sanz, P., Belt, S.T. (2014). Holocene sub-centennial
602 evolution of Atlantic water inflow and sea ice distribution in the western Barents Sea.
603 *Climate of the Past* 10, 181–198.
604 Bauch, H.A., Erlenkeuser, H., Spielhagen, R.F., Struck, U., Matthiessen, J., Thiede, J.,
605 Heinemeier, J. (2001). A multiproxy reconstruction of the evolution of deep and surface
606 waters in the subarctic Nordic seas over the last 30,000 yr. Quaternary Science Reviews
607 20, 659–678.

608 Birks, C.J.A., Koç, N. (2002). A high-resolution diatom record of late quaternary sea-surface
609 temperatures and oceanographic conditions from the eastern Norwegian Sea. Boreas 31,
610 323–344.
611 Brice, C., de Vernal, A., Ivanova, E., van Bellen, S., & Van Nieuwenhove, N. (2020).
612 Palynological evidence of sea-surface conditions in the Barents Sea off northeast Svalbard
613 during the postglacial period. *Quaternary Research*, 1-15.
614 Cage, A. G., Pieńkowski, A. J., Jennings, A., Knudsen, K. L., & Seidenkrantz, M. S. (2021).
615 Comparative analysis of six common foraminiferal species of the genera Cassidulina,
616 Paracassidulina, and Islandiella from the Arctic–North Atlantic domain. *Journal of*
617 *Micropalaeontology*, *40*(1), 37-60.
618 Calvo, E., Grimalt, J., Jansen, E. (2002). High resolution U37K sea surface temperature
619 reconstruction in the Norwegian Sea during the Holocene. Quaternary Science Reviews
620 21, 1385–1394.
621 Caralp, M.H. (1989). Abundance of Bulimia exilis and Melonis barleeanum: relationship to the
622 quality of marine organic matter. Geo-Marine Letters 9, 37–43.
623 Carbonara, K., Mezgec, K., Varagona, G., Musco, M. E., Lucchi, R. G., Villa, G., Morigi, C.,
624 Melis, R., & Caffau, M. (2016). Palaeoclimatic changes in Kveithola, Svalbard, during the
625 Late Pleistocene deglaciation and Holocene: Evidence from microfossil and sedimentary
626 records. *Palaeogeography, Palaeoclimatology, Palaeoecology*, *463*, 136-149.
627 Chauhan, T., Rasmussen, T. L., & Noormets, R. (2016). Palaeoceanography of the Barents Sea
628 continental margin, north of Nordaustlandet, Svalbard, during the last 74 ka. *Boreas*, *45*(1),
629 76-99.
630 Chistyakova, N., Ivanova, E., Risebrobakken, B., Ovsepyan, E., Ovsepyan, Y. (2010).
631 Reconstruction of the postglacial environments in the southwestern Barents Sea based on
632 foraminiferal assemblages. *Oceanology* 50, 573–581.
633 Cohen, J., Screen, J. A., Furtado, J. C., Barlow, M., Whittleston, D., Coumou, D., Francis, J.,
634 Dethloff, K., Entekhabi, D., Overland, J., & Jones, J. (2014). Recent Arctic amplification
635 and extreme mid-latitude weather. *Nature geoscience*, *7*(9), 627.
636 Cottier, F., Tverberg, V., Inall, M., Svendsen, H., Nilsen, F., & Griffiths, C. (2005). Water
637 mass modification in an Arctic fjord through cross-shelf exchange: The seasonal
638 hydrography of Kongsfjorden, Svalbard. *Journal of Geophysical Research:*
639 *Oceans*, *110*(C12).
640 Corliss, B. H. (1991). Morphology and microhabitat preferences of benthic foraminifera from
641 the northwest Atlantic Ocean. *Marine micropaleontology*, *17*(3-4), 195-236.

642 Darling, K. F., Schweizer, M., Knudsen, K. L., Evans, K. M., Bird, C., Roberts, A., Filipsson,
643 H. L., Kim, J-H., Gudmundsso, G., Wade, C., Sayer, M. D. J. & Austin, W. E. (2016). The
644 genetic diversity, phylogeography and morphology of Elphidiidae (Foraminifera) in the
645 Northeast Atlantic. *Marine Micropaleontology*, *129*, 1-23.
646 de Vernal, A., Rochon, A., Fréchette, B., Henry, M., Radi, T., Solignac, S. (2013).
647 Reconstructing past sea ice cover of the Northern Hemisphere from dinocyst assemblages:
648 status of the approach. *Quaternary Science Reviews* 79, 122–134.
649 Dowdeswell, J.A., Whittington, R.J., Jennings, A.E., Andrews, J.T., Mackensen, A. &
650 Marienfeld, P. (2000). An origin for laminated glacimarine sediments through sea-ice
651 build-up and suppressed iceberg rafting. Sedimentology 47, 557-576.
652 Dowdeswell, J.A., Hogan, K.A., Evans, J., Noormets, R., Ó'Cofaigh, C., Ottesen, D. (2010).
653 Past ice-sheet flow east of Svalbard inferred from streamlined subglacial landforms.
654 Geology 38, 163e166.
655 Dreimanis, A. (1976), Tills: Their Origin and Properties: Glacial Till, An Inter-disciplinary
656 study, The Royal Society of Canada Special Publications, No. 12, (Robert F, Leget) p. 15.
657 Duplessy, J.-C., Ivanova, E., Murdmaa, I., Paterne, M., Labeyrie, L. (2001). Holocene
658 paleoceanography of the Northern Barents Sea and variations of the northward heat
659 transport by the Atlantic Ocean. Boreas 30, 2–16.
660 Eldevik, T., Risebrobakken, B., Bjune, A.E., Andersson, C., Birks, H.J.B., Dokken, T.M.,
661 Drange, H., et al. (2014). A brief history of climate – the northern seas from the Last Glacial
662 Maximum to global warming. *Quaternary Science Reviews* 106, 225–246.
663 Elverhøi, A., & Solheim, A. (1983). The Barents Sea ice sheet-a sedimentological
664 discussion. *Polar research*, *1*(1), 23-42.
665 Elverhøi, A, Lønne, Ø & Seland, R (1983) Glaciomarine sedimentation in a modern fjord
666 environment, Spitsbergen. Polar Research, 1(2), 127–150.
667 Elverhøi, A., & Lauritzen, Ø. (1984). Bedrock geology of the northern Barents Sea (west of 35
668 E) as inferred from the overlying Quaternary deposits. *Skrifter-Norsk Polarinstitutt*, (180),
669 5-16.
670 Fatela, F., Taborda, R. (2002). Confidence limits of species proportions in microfossil
671 assemblages. Marine Micropaleontology 45, 169–174.
672 Feyling-Hanssen, R. W. (1964). A marine section from the Holocene of Talavera on
673 Barentsdya in Spitsbergen, with a record of the Foraminifera. Vorttlige des Fridtjof-
674 Nansen-Gediichmk-Symposiom ilber Spitsbergen 3-11 April 1961 im Wilrzburg, 30-58.
675 Steiner Verlag, Wiesbaden (Nor. Polar- insr. Medd. 93, Oslo 1965).

676 Forman Steven L., Polyak Leonid (1997) Radiocarbon content of pre-bomb marine mollusks
677 and variations in the14C Reservoir age for coastal areas of the Barents and Kara Seas,
678 Russia. Geophysical Research Letters, 24, (8), 885. –
679 888. http://dx.doi.org/10.1029/97gl00761
680 Fransner, O., Noormets, R., Flink, A. E., Hogan, K. A., O'Regan, M., & Jakobsson, M. (2017).
681 Glacial landforms and their implications for glacier dynamics in Rijpfjorden and
682 Duvefjorden, northern Nordaustlandet, Svalbard. *Journal of Quaternary Science*, *32*(3),
683 437-455.
684 Groot, D. E., Aagaard-Sørensen, S., & Husum, K. (2014). Reconstruction of Atlantic water
685 variability during the Holocene in the western Barents Sea. *Climate of the Past*, *10*(1), 51-
686 62.
687 Hagen, JO, Liestøl, O, Roland, ERIK & Jørgensen, T(1993) Glacier atlas of Svalbard and jan
688 mayen. 129 Oslo: Norsk Polarinstitutt., 141.
689 Hald, M., Vorren, T.O. (1987). Foraminiferal stratigraphy and environment of late Weichselian
690 deposits on the continental shelf off Troms, Northern Norway. Marine Micropaleontology
691 12 (2), 129–160.
692 Hald, M, Steinsund, Pi, Dokken, T, Korsun, S, Polyak, L & Aspeli, R (1994) Recent and late
693 quaternary distribution of elphidium excavatumf. clavatumin arctic seas. Cushman
694 Foundation for Foraminiferal Research, 141,
695 Hald, M., & Aspeli, R. (1997). Rapid climatic shifts of the northern Norwegian Sea during the
696 last deglaciation and the Holocene. *Boreas*, *26*(1), 15-28.
697 Hald, M., Korsun, S. (1997). Distribution of modern benthic foraminifera from fjords of
698 Svalbard, European Arctic. Journal of Foraminiferal Research 27, 101–122.
699 Hald Morten, Dahlgren Torbjörn, Olsen Tor-Eirik, Lebesbye Erland (2001) Late Holocene
700 palaeoceanography in Van Mijenfjorden, Svalbard. Polar Research, 20, (1), 23. –
701 35. http://dx.doi.org/10.3402/polar.v20i1.6497
702 Hald, M., Ebbesen, H., Forwick, M., Godtliebsen, F., Khomenko, L., Korsun, S., Olsen, L.R.,
703 Vorren, T.O. (2004). Holocene Paleoceanography and glacial history of the West
704 Spitsbergen area, Euro-Arctic margin. Quaternary Science Reviews 23, 2075–2088.
705 Hald Morten, Andersson Carin, Ebbesen Hanne, Jansen Eystein, Klitgaard-
706 Kristensen Dorthe, Risebrobakken Bjørg, Salomonsen GauteR., Sarnthein Michael, Sejrp
707 Hans Petter, Telford Richard J. (2007) Variations in temperature and extent of Atlantic
708 Water in the northern North Atlantic during the Holocene. Quaternary Science
709 Reviews, 26, (25-28), 3423. –3440. http://dx.doi.org/10.1016/j.quascirev.2007.10.005

Harland, W. B., Wallis, R. H., & Gayer, R. A. (1966). A revision of the lower Hecla Hoek succession in central north Spitsbergen and correlation elsewhere. *Geological Magazine*, *103*(1), 70-97.

Hayward, B.W.; Le Coze, F.; Vachard, D.; Gross, O. (2021). World Foraminifera Database. Accessed at http://www.marinespecies.org/foraminifera on 2021-04-09. doi:10.14284/305

Heaton, T. J., Köhler, P., Butzin, M., Bard, E., Reimer, R. W., Austin, W. E., Ramsey, C. B., Grootes, P. M., Hughen, K. A., Kromer, B., Riemer, P. J., Adkins, J., Burke, A., Cook, M. S., Olsen, J., & Skinner, L. C. (2020). Marine20—the marine radiocarbon age calibration curve (0–55,000 cal BP). *Radiocarbon*, *62*(4), 779-820.

Helland-Hansen, B., & Nansen, F. (1909). *The Norwegian Sea: its physical oceanography based upon the Norwegian researches 1900-1904*. Det Mallingske bogtrykkeri.

Hogan, K. A., Dowdeswell, J. A., Noormets, R., Evans, J., Cofaigh, C. Ó., & Jakobsson, M. (2010). Submarine landforms and ice-sheet flow in the Kvitøya Trough, northwestern Barents Sea. *Quaternary Science Reviews*, *29*(25-26), 3545-3562.

Hop, H., Assmy, P., Wold, A., Sundfjord, A., Daase, M., Duarte, P., Kwasniewski, S., Gluchowska, M., Wiktor, J. M., Tatarek, A., Wiktor, J. Jr., Kristiansen, S., Fransson, A., Chierici, M., & Vihtakari, M. (2019). Pelagic ecosystem characteristics across the Atlantic water boundary current from Rijpfjorden, Svalbard, to the Arctic Ocean during summer (2010–2014). *Frontiers in Marine Science*, *6*, 181.

Hopkins, T. S. (1991). The GIN Sea—A synthesis of its physical oceanography and literature review 1972–1985. *Earth-Science Reviews*, *30*(3-4), 175-318.

Hormes, A., Akcar, N., & Kubik, P. W. (2011). Cosmogenic radionuclide dating indicates ice-sheet configuration during MIS 2 on Nordaustlandet, Svalbard. *Boreas*, *40*(4), 636-649.

Hormes A., Før Gjermundsen E., Rasmussen T. L. (2013). From mountain top to the deep sea - Deglaciation in 4D of the northwestern Barents Sea ice sheet. Quaternary Science Reviews 75, 78-99.

Huthnance, J. M. (1991). Physical oceanography of the North Sea. *Ocean and shoreline management*, *16*(3-4), 199-231.

Ivanova, E., Murdmaa, I., de Vernal, A., Risebrobakken, B., Peyve, A., Brice, C., Seitkalieva, E. & Pisarev, S. (2019). Postglacial paleoceanography and paleoenvironments in the northwestern Barents Sea. *Quaternary Research*, *92*(2), 430-449.

Jessen, S.P., Rasmussen, T.L., Nielsen, T., Solheim, A. (2010). A new Late Weichselian and Holocene marine chronology for the western Svalbard slope 30,000-0. Cal years BP. Quaternary Science Reviews 29, 1301e1312

744 Johansson, Å., Maluski, H., & Gee, D. G. (2001). Ar-Ar dating of Caledonian and Grenvillian
745 rocks from northeasternmost Svalbard-evidence of two stages of Caledonian
746 tectonothermal activity in the high Arctic?. *Norwegian Journal of Geology/Norsk*
747 *Geologisk Forening*, *81*(4).
748 Krasil'Ščikov, A. A., Kubanskij, A. P., & Ohta, Y. (1995). Surface magnetic anomaly study on
749 the eastern part of the Forlandsundet Graben. *Polar Research*, *14*(1), 55-68.
750 Kristensen, D. K., Rasmussen, T. L., & Koç, N. (2013). Palaeoceanographic changes in the
751 northern B arents S ea during the last 16 000 years–new constraints on the last deglaciation
752 of the S valbard–B arents S ea I ce S heet. *Boreas*, *42*(3), 798-813.
753 Koç, N., Klitgaard Kristensen, D., Hasle, K., Forsberg, C.F., Solheim, A. (2002). Late glacial
754 paleoceanography of Hinlopen Strait, northern Svalbard. Polar Research 21, 307–314.
755 Korsun, S.A., Polyak, L.V. (1989). Distribution of benthic foraminiferal morphogroups in the
756 Barents Sea. Oceanology 29 (USSR), 838–844.
757 Korsun, S., & Hald, M. (1998). Modern benthic foraminifera off Novaya Zemlya tidewater
758 glaciers, Russian Arctic. *Arctic and Alpine Research*, *30*(1), 61-77.
759 Korsun, S., Hald, M., Golikova, E., Yudina, A., Kuznetsov, I., Mikhailov, D., & Knyazeva, O.
760 (2014). Intertidal foraminiferal fauna and the distribution of Elphidiidae at Chupa Inlet,
761 western White Sea. *Marine Biology Research*, *10*(2), 153-166.
762 Kubischta, F., Knudsen, K.L., Ojala, A.E.K., Salonen, V.-P. (2011). Holocene benthic
763 foraminiferal record from a high-Arctic fjord, Nordaustlandet, Svalbard. Geografiska
764 Annaler: Series A, Physical Geography 93, 227e242.
765 Leu, E, Søreide, JE, Hessen, DO, Falk-Petersen, S and Berge, J (2011). Consequences of
766 changing sea-ice cover for primary and secondary producers in the European Arctic shelf
767 seas: timing, quantity and quality. *Progr. Oceanogr.*, 90(1–4), 18–32 (doi:
768 10.1016/j.pocean.2011.02.004)
769 Lloyd, J. M. (2006). Modern distribution of benthic foraminifera from Disko Bugt, West
770 Greenland. *Journal of Foraminiferal Research*, *36*(4), 315-331.
771 Locarnini RA, Mishonov AV, Baranova OK, Boyer, TP, Zweng, MM, Garcia, HE, Reagan, J
772 R, Seidov, D, Weathers, KW, Paver, CR & Smolyar, IV 2019. World Ocean Atlas
773 2018, Volume 1: Temperature. A. Mishonov, Technical Editor. NOAA Atlas NESDIS 81,
774 52pp.
775 Lubinski, D. J., Forman, S. L., & Miller, G. H. (1999). Holocene glacier and climate
776 fluctuations on Franz Josef Land, Arctic Russia, 80 N. *Quaternary Science Reviews*, *18*(1),
777 85-108.

778 Lubinski, D.J., Polyak, L., Forman, S.L. (2001). Freshwater and Atlantic water inflows to the
779 deep northern Barents and Kara seas since ca 13 14C ka: foraminifera and stable isotopes.
780 *Quaternary Science Reviews* 20, 1851–1879.
781 Lo Giudice Cappelli, E., & Austin, W. E. N. (2019). Marine bivalve feeding strategies and
782 radiocarbon ages in Northeast Atlantic coastal waters. *Radiocarbon*.
783 Manabe, S., & Stouffer, R. J. (1980). Sensitivity of a global climate model to an increase of
784 CO2 concentration in the atmosphere. *Journal of Geophysical Research:*
785 *Oceans*, *85*(C10), 5529-5554.
786 Mangerud J., Bondevik S., Gulliksen S., Hufthammer Anne, Høisæter Tore (2006) Marine
787 14C reservoir ages for 19th century whales and molluscs from the North
788 Atlantic. Quaternary Science Reviews, 25, (23-24), 3228. –
789 3245. http://dx.doi.org/10.1016/j.quascirev.2006.03.010
790 Manley, T. O. (1995). Branching of Atlantic Water within the Greenland-Spitsbergen passage:
791 An estimate of recirculation. *Journal of Geophysical Research: Oceans*, *100*(C10), 20627-
792 20634.
793 Mudie, P.J., Keen, C.E., Hardy, I.A. & Vilks, G. (1984). Multivariate-analysis and quantitative
794 paleoecology of benthic foraminifera in surface and late Quaternary shelf sediments,
795 northern Canada. Marine Micropaleontology 8, 283– 313.
796 Müller, J., Werner, K., Stein, R., Fahl, K., Moros, M., Jansen, E. (2012). Holocene cooling
797 culminates in sea ice oscillations in Fram Strait. *Quaternary Science Reviews* 47, 1–14.
798 Müller, J., & Stein, R. (2014). High-resolution record of late glacial and deglacial sea ice
799 changes in Fram Strait corroborates ice–ocean interactions during abrupt climate
800 shifts. *Earth and Planetary Science Letters*, *403*, 446-455.
801 Murray, J. W. (1991). Ecology and distribution of benthic foraminifera. *Biology of*
802 *foraminifera*, 221-254.
803 Murray, J. W. (2006). *Ecology and applications of benthic foraminifera*. Cambridge university
804 press.
805 Nielsen, T., & Rasmussen, T. L. (2018). Reconstruction of ice sheet retreat after the Last
806 Glacial maximum in Storfjorden, southern Svalbard. *Marine Geology*, *402*, 228-243.
807 Otto, L., Zimmerman, J. T. F., Furnes, G. K., Mork, M., Saetre, R., & Becker, G. (1990).
808 Review of the physical oceanography of the North Sea. *Netherlands journal of sea*
809 *research*, *26*(2-4), 161-238.

Pawłowska, J., Łącka, M., Kucharska, M., Pawlowski, J., & Zajączkowski, M. (2020). Multiproxy evidence of the Neoglacial expansion of Atlantic Water to eastern Svalbard. *Climate of the Past*, *16*(2), 487-501.

Pfirman, S., Bauch, D., & Gammelsrød, T. (1994). The northern Barents Sea: water mass distribution and modification. AGU, Ameircan Geophysical Union.

Pieńkowski, A. J., Husum, K., Belt, S. T., Ninnemann, U., Köseoğlu, D., Divine, D. V., L. Smik, J. Knies, K. Hogan & Noormets, R. (2021). Seasonal sea ice persisted through the Holocene Thermal Maximum at 80 N. *Communications Earth & Environment*, *2*(1), 1-10.

Plassen Liv, Vorren Tore O., Forwick Matthias (2004) Integrated acoustic and coring investigation of glacigenic deposits in Spitsbergen fjords. Polar Research, 23, (1), 89. – 110. http://dx.doi.org/10.1111/j.1751-8369.2004.tb00132.x

Polyak, L., Solheim, A. (1994). Late- and postglacial environments in the northern Barents Sea west of Franz Josef Land. Polar Research 13, 197–207.

Polyak, L., & Mikhailov, V. (1996). Post-glacial environments of the southeastern Barents Sea: foraminiferal evidence. *Geological Society, London, Special Publications*, *111*(1), 323-337.

Powell, R. D. (1984). Glacimarine processes and inductive lithofacies modelling of ice shelf and tidewater glacier sediments based on Quaternary examples. *Marine Geology*, *57*(1-4), 1-52.

Rasmussen, T.L., Thomsen, E., Ślubowska, M.A., Jessen, S., Solheim, A., Koç, N. (2007). Paleoceanographic evolution of the SW Svalbard margin (76°N) since 20,000 14C yr BP. Quaternary Research 67, 100–114.

Rasmussen, T. L., Forwick, M., & Mackensen, A. (2012). Reconstruction of inflow of Atlantic Water to Isfjorden, Svalbard during the Holocene: Correlation to climate and seasonality. *Marine Micropaleontology*, *94*, 80-90.

Rasmussen, S. O., Bigler, M., Blockley, S. P., Blunier, T., Buchardt, S. L., Clausen, H. B., Cvijanovic, I., Dahl-Jensen, D., Johnsen, S. J., Fischer, H., Gkinis, V., Guillevic, M., Hoek, W. H., Lowe, J., Pedro, J. B., Popp, H., Seierstad, I. K., Steffensen, J. P., Svensson, A. M., Vallelonga, P., Vinther, B. M., Walker, M. J. C., Wheatley, J. J., and Winstrup, M. (2014). A stratigraphic framework for abrupt climatic changes during the Last Glacial period based on three synchronized Greenland ice-core records: refining and extending the INTIMATE event stratigraphy. *Quaternary Science Reviews*, *106*, 14-28.

Rasmussen Tine L., Thomsen Erik (2021) Climate and ocean forcing of ice-sheet dynamics along the Svalbard-Barents Sea ice sheet during the deglaciation ~20,000–10,000 years

BP. Quaternary Science Advances, 3, 100019. http://dx.doi.org/10.1016/j.qsa.2020.100019

Rigual-Hernández, A. S., Colmenero-Hidalgo, E., Martrat, B., Bárcena, M. A., de Vernal, A., Sierro, F. J., Flores, J. A., Grimalt, J.O., Henry, M., and Lucchi, R. G. (2017). Svalbard ice-sheet decay after the Last Glacial Maximum: New insights from micropalaeontological and organic biomarker paleoceanographical reconstructions. *Palaeogeography, Palaeoclimatology, Palaeoecology*, *465*, 225-236.

Risebrobakken, B., Moros, M., Ivanova, E. V., Chistyakova, N., & Rosenberg, R. (2010). Climate and oceanographic variability in the SW Barents Sea during the Holocene. *The Holocene*, *20*(4), 609-621.

Risebrobakken, B., Dokken, T., Smedsrud, L. H., Andersson, C., Jansen, E., Moros, M., & Ivanova, E. V. (2011). Early Holocene temperature variability in the Nordic Seas: The role of oceanic heat advection versus changes in orbital forcing. *Paleoceanography*, *26*(4).

Risebrobakken, B., & Berben, S. M. (2018). Early holocene establishment of the barents sea Arctic front. *Frontiers in Earth Science*, *6*, 166.

Rudels B. 1987. On the mass balance of the Polar Ocean, with special emphasis on the Fram Strait. NORSK POLARINSTITUTT OSLO

Rudels, B., Friedrich, H. J., & Quadfasel, D. (1999). The Arctic circumpolar boundary current. *Deep Sea Research Part II: Topical Studies in Oceanography*, *46*(6-7), 1023-1062.

Rytter F. (2002) MODERN DISTRIBUTION OF BENTHIC FORAMINIFERA ON THE NORTH ICELANDIC SHELF AND SLOPE. The Journal of Foraminiferal Research, 32, (3), 217. –244. http://dx.doi.org/10.2113/32.3.217

Saloranta, T. M., & Haugan, P. M. (2001). Interannual variability in the hydrography of Atlantic water northwest of Svalbard. *Journal of Geophysical Research: Oceans*, *106*(C7), 13931-13943.

Salvigsen, 0., Forman, S. L. & Miller, G. H. (1992). Thermophilous molluscs on Svalbard during the Holocene and their paleoclimatic implications. *Polar Research* 11(1), 1-10

Salvigsen, O. (2002). Radiocarbon-date d Mytilus edulis and Modiolus modiolus from northern Svalbard: climatic implications. *Norsk Geografisk Tidsskrift–Norwegian Journal of Geography* Vol. 56, 56–61. Oslo. ISSN 0029-1951.

Sarnthein, M., Pflaumann, U., Weinelt, M. (2003). Past extent of sea ice in the northern North Atlantic inferred from foraminiferal paléotempératures estimates. Paleoceanography 18, 1047.

878 Schlichtholz Pawel, Goszczko Ilona (2006) Interannual variability of the Atlantic water layer
879 in the West Spitsbergen Current at in summer 1991–2003. Deep Sea Research Part I:
880 Oceanographic Research Papers, 53, (4), 608. –
881 626. http://dx.doi.org/10.1016/j.dsr.2006.01.001
882 Serreze, M. C., & Francis, J. A. (2006). The Arctic amplification debate. *Climatic*
883 *change*, *76*(3-4), 241-264.
884 Serreze, M. C., Barrett, A. P., Stroeve, J. C., Kindig, D. N., & Holland, M. M. (2009). The
885 emergence of surface-based Arctic amplification. *The Cryosphere*, *3*(1), 11-19.
886 Skirbekk, K., Kristensen, D. K., Rasmussen, T. L., Koç, N., & Forwick, M. (2010). Holocene
887 climate variations at the entrance to a warm Arctic fjord: evidence from Kongsfjorden
888 trough, Svalbard. *Geological Society, London, Special Publications*, *344*(1), 289-304.
889 Ślubowska, M.A., Koç, N., Rasmussen, T.L., Klitgaard Kristensen, D. (2005). Changes in the
890 flow of Atlantic water into the Arctic Ocean since the last deglaciation: evidence from the
891 northern Svalbard continental margin, 80°N. Paleoceanography 20, 4014.
892 Ślubowska-Woldengen, M., Rasmussen, T.L., Koç, N., Klitgaard Kristensen, D., Nilsen, F.,
893 Solheim, A. (2007). Advection of Atlantic Water to the western and northern Svalbard
894 shelf since 17,500 cal yr BP. Quaternary Science Reviews 26, 463–478.
895 Streeter, S. S. (1980). Oxygen isotope ratios in foraminifera. *Paleobiology*, *6*(1), 3-4.
896 Steinsund, P.I., Polyak, L., Hald, M., Mikhailov, V., Korsun, S. (1994). Benthic foraminifera
897 in surface sediments of the Barents and Kara seas. In: Steinsund, P.I. (Ed.), Benthic
898 foraminifera in Surface Sediments of the Barents and Kara Seas: Modern and Late
899 Quaternary Applications. Ph.D. Thesis, University of Tromsø, Norway, pp. 61–102.
900 Steinsund, P. I. (1994). Benthic foraminifera in surface sediments of the Barents and Kara seas:
901 modern and late Quaternary applications. PhD diss., Institute of Biology and Geology,
902 Department of Geology, University of Tromsø, Tromsø, Norway.
903 Sternal, B., Szczucińs ki, W., Forwick, M., Zajaczkowski, M., Lorenc, S., Przytarska, J. (2014).
904 Postglacial variability in nearbottom current speed on the continental shelf off south-west
905 Spitsbergen. *Journal of Quaternary Science* 29, 767–777.
906 Stuiver, M., Reimer, P.J., and Reimer, R.W. (2021). CALIB 8.2; http://calib.org, accessed
907 2021-4-9
908 Telesiński, M. M., Bauch, H. A., Spielhagen, R. F., & Kandiano, E. S. (2015). Evolution of the
909 central Nordic Seas over the last 20 thousand years. *Quaternary Science Reviews*, *121*, 98-
910 109.

911 Vilks G. 1980. Postglacial basin sedimentation on Labrador Shelf. GEOL. SURV. CANADA,
912 PAPER; NO 78-28; 28 P
913 Walker, M., Johnsen, S., Rasmussen, S. O., Popp, T., Steffensen, J.-P., Gibbard, P., Hoek, W.,
914 Lowe, J., Andrews, J., Björck, S., Cwynar, L. C., Hughen, K., Kershaw, P., Kromer, B.,
915 Litt, T., Lowe, D. J., Nakagawa, T., Newnham, R., and Schwander, J. (2009). Formal
916 definition and dating of the GSSP (Global Stratotype Section and Point) for the base of the
917 Holocene using the Greenland NGRIP ice core and selected auxiliary records. *Journal of*
918 *Quaternary Science: Published for the Quaternary Research Association*, *24*(1), 3-17.
919 Werner, K., Spielhagen, R;F., Bauch, D., Hass, H.C., Kandiano, E.S., Zamelczyk,
920 K. (2011). Atlantic Water advection to the eastern Fram Strait - multiproxy evidence for
921 late Holocene variability. *Palaeogeography, Palaeoclimatology, Palaeoecology,* 308 (3-
922 4), 264-276.
923 Werner, K., Spielhagen, R. F., Bauch, D., Hass, H. C., & Kandiano, E. (2013). Atlantic Water
924 advection versus sea-ice advances in the eastern Fram Strait during the last 9 ka:
925 Multiproxy evidence for a two-phase Holocene. *Paleoceanography*, *28*(2), 283-295.
926 Werner, K., Müller, J., Husum, K., Spielhagen, R. F., Kandiano, E. S., & Polyak, L. (2016).
927 Holocene sea subsurface and surface water masses in the Fram Strait–Comparisons of
928 temperature and sea-ice reconstructions. *Quaternary Science Reviews*, *147*, 194-209.
929 Wollenburg, J. E., Knies, J., & Mackensen, A. (2004). High-resolution paleoproductivity
930 fluctuations during the past 24 kyr as indicated by benthic foraminifera in the marginal
931 Arctic Ocean. *Palaeogeography, palaeoclimatology, palaeoecology*, *204*(3-4), 209-238.
932 Zweng MM, Reagan JR, Seidov T, Boyer, RA, Locarnini, HE, Garcia, AV, Mishonov, OK, B
933 aranova, KW, Weathers, CR, Paver, CR & Smolyar, IV . 2019. World ocean atlas 2018,
934 Volume 2: Salinity. A. Mishonov, Technical Editor, NOAA Atlas NESDIS 82, 50pp.

Acknowledgements

All the authors grateful to the reviewers and the associate editor for their comments and suggestions, which have been very helpful in improving the original manuscript. MP thanks the ERASMUS + program for the financial support during her secondment at the University of St Andrews.

940 Table 1: Conventional and calibrated radiocarbon age results, including details of the
941 laboratory code, core depth, median probability age and dating material pictures

Reference number	Core depth (cm)	^{14}C age Age ± 1σ (years)	^{14}C age Calibrated years BP (2σ)	Median Probability (Cal. year BP)	Material	
UBA-25663	8 – 9	811 ± 29	3 - 328	194	Bivalve shells	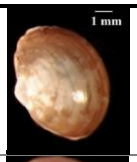
UBA-25664	75 – 77	9 256 ± 49	9529 - 9969	9744	*Nonionellina labradorica*	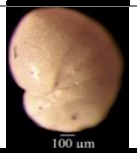
UBA-25666	134 – 138	10 403 ± 54	11134 - 11587	11318		
UBA-25667	171 – 179	9 855 ± 51	10307 - 10770	10557		

942

943 Table 2: Summary of the environmental preferences of the most common foraminifera species
944 in the core HH12-04-GC

	Ecology												
Species & identification references	Arctic front	Glaciomarine	Atlantic water	Arctic	Younger Dryas	Low salinities	High salinity	Productivity	Organic matter	Sea ice cover	Glacier termini	Glaciers & ice caps	Open ocean	Strong currents	**References**
Cassidulina reniforme Nørvang, 1945		X								X					Hald & Korsun, 1997; Hald & Vorren, 1987
Elphidium clavatum Cushman, 1944		X									X				Hald et al., 1994; Elverhøi et al., 1983; Darling et al., 2016
Elphidium asklundi Brotzen, 1943		X										X			Austin, 1991; Polyak & Solheim, 1994
Elphidium albiumbilicatum Weiss, 1954			X			X									Alve & Murray, 1999; Korsun et al., 2014
Islandiella norcrossi Cushman, 1933			X				X	X							Hald & Korsun, 1997; Streeter, 1980; Lloyd, 2006; Cage et al., 2021
Nonionellina labradorica Dawson, 1860	X								X						Vilks, 1980; Mudie et al., 1984; Corliss, 1991
Melonis barleeanum Dawson, 1860			X						X						Caralp, 1989; Korsun and Polyak, 1989
Cibicides lobatulus Walker & Jacob, 1798			X										X		Murray, 1991, 2006; Steinsund et al., 1994
Islandiella helenae Feyling-Hanssen & Buzas, 1976				X				X			X				Hald & Korsun, 1997; Wollenburg et al., 2004; Cage et al., 2021
Buccella tenerrima Bandy, 1950				X				X		X					Mudie et al., 1984; Polyak and Solheim, 1994
Cribrostomoides crassimargo Feyling-Hanssen, 1954				X									X		Lloyd, 2006
Stainforthia loeblichi Feyling-Hanssen, 1954				X						X					Steinsund, 1994
Stainforthia fusiformis Williamson, 1858					X	X									Feyling-Hanssen, 1964

945

Figures captions:

Figure 1: Location of the study core HH12-04-GC in Riipfjorden (Nordaustlandet), with the main current systems in the Nordic seas and Polar region from Atlantic or Arctic origins

Plate 1: Light microscope images of dominant species: a. *Cassidulina reniforme* (lateral view), b and c. *Elphidium clavatum* (lateral view), d. *Elphidium asklundi* (lateral view), e. *Elphidium albiumbilicatum* (lateral view), f. *Islandiella helenae* (lateral view), g. *Islandiella norcrossi* (lateral view) and h. *Melonis barleeanum* (lateral view)

Plate 2: Light microscope images of dominant species: a. *Cibicides lobatulus* (dorsal view); b. *Cibicides lobatulus* (ventral view); c *Nonionellina labradorica* (lateral view), d. *Nonionellina labradorica* (oblique lateral view) and e. *Nonionellina labradorica* (apertural view); f. *Buccella tenerrima* (dorsal view), g. *Neogloboquadrina pachyderma* (ventral view); h and i. *Stainforthia fusiformis* (side views), j. *Stainforthia loeblichi* (apertural view); and k. *Cribrostomoides crassimargo* (lateral view).

Figure 2: Lithological data including the LOG of the core HH12-04-GC, the grain size on the fraction 1 mm (both from Fransner et al., 2017), the concentration of >2mm clasts and pictures of the clasts of 3 different stratigraphical levels. Three lithological zonation are defined and interpretated. The ^{14}C dates are reported in cal. yrs BP

Figure 3: Faunal diagram of the core HH12-04-GC, showing the abundance of the dominant-foraminifer species and the faunal zonation. Ecological interpretations are reported following the information in Table 2. The ^{14}C dates are reported in cal. yrs BP

Figure 4: Synthesis plot with the log of core HH12-04-GC, the concentration of >2mm clasts and 6 key indicators species, such as *S. fusiformis* (as dating indicator of the deglaciation), *C. reniforme* (as glaciomarine indicator), *C. lobatulus, M. barleeanum* and *N. labradorica* (respectively as strong current velocity, high productivity and presence of Arctic front) and *B. tenerrima* (as an Artic species). These data are compared with IRD flux from core JM02-440 (Ślubowska-Woldengen et al., 2007) and benthic foraminiferal concentration from cores JM02-440 (Ślubowska-Woldengen et al., 2007), JM98-845 (Rasmussen et al., 2012), JM02-460 (Rasmussen et al., 2007), NP94-51 (Ślubowska et al., 2005) and NP05-21 (Skirbekk et al., 2010). The black lines correspond to the correlation of radiocarbon dating with previously published data. The dotted line is the line of radiocarbon dates that may have been affected by a reversal. The ^{14}C dates are reported in cal. yrs BP

Figure 5: Interrelated schema of paleoenvironmental and palaeoceanographic evolutions (sea-ice cover and Arctic front) at HH12-04-GC core site throughout postglacial time. Dashed lines at Riipfjorden have been placed for illustrative purposes only

Figure SM1: graphics representing the number of foraminifera against the number of species for five different samples. This allows to define the minimum number of specimens that should be counted, according to Fatela and Taborda (2002)

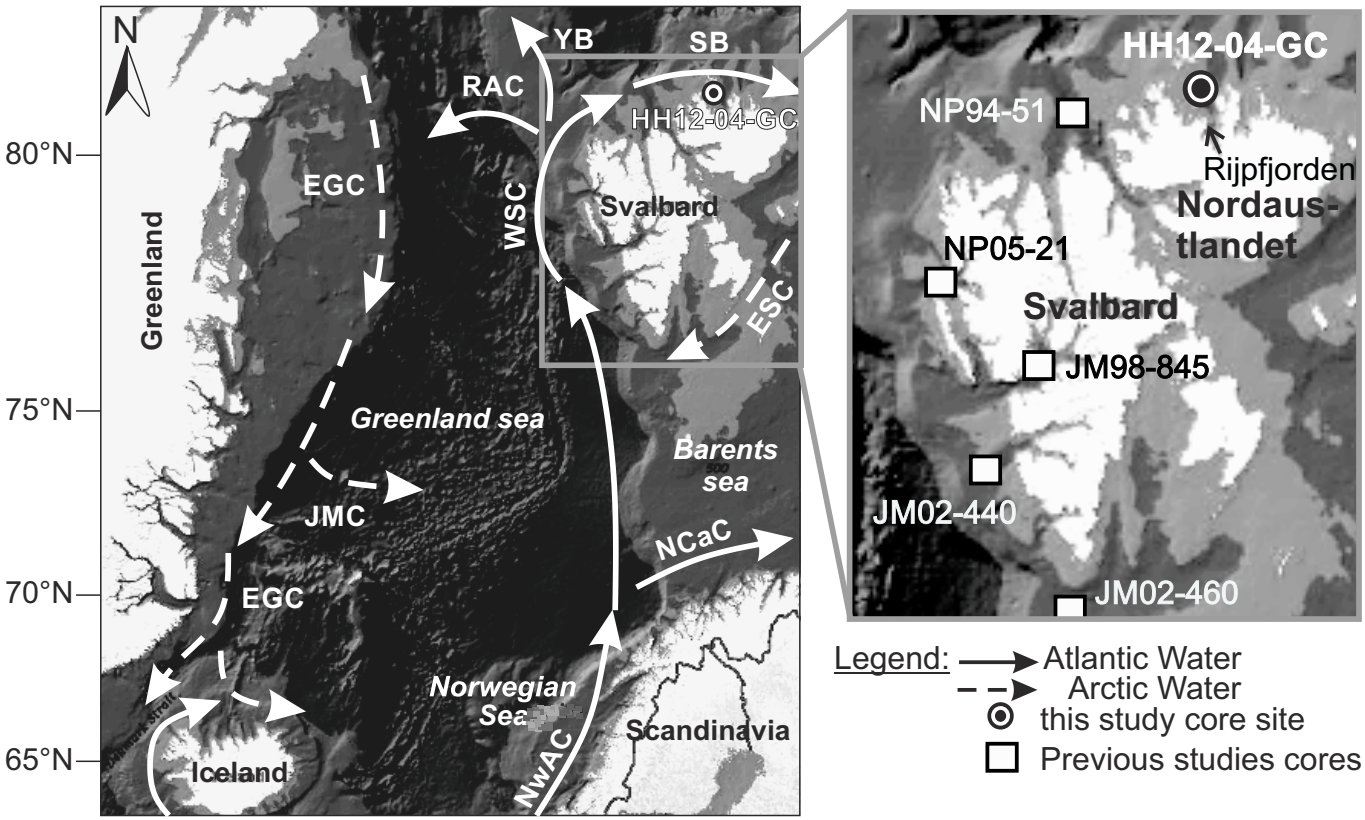

NwAC: Norwegian Atlantic Current
NCaC: North Cape Current
WSC: West Spitsbergen Current

ESC: East Spitsbergen Current
SB: Svalbard Branch
YB: Yermak Branch

RAC: Return Atlantic Current
EGC: East Greenland Current
JMC: Jan Mayen Current

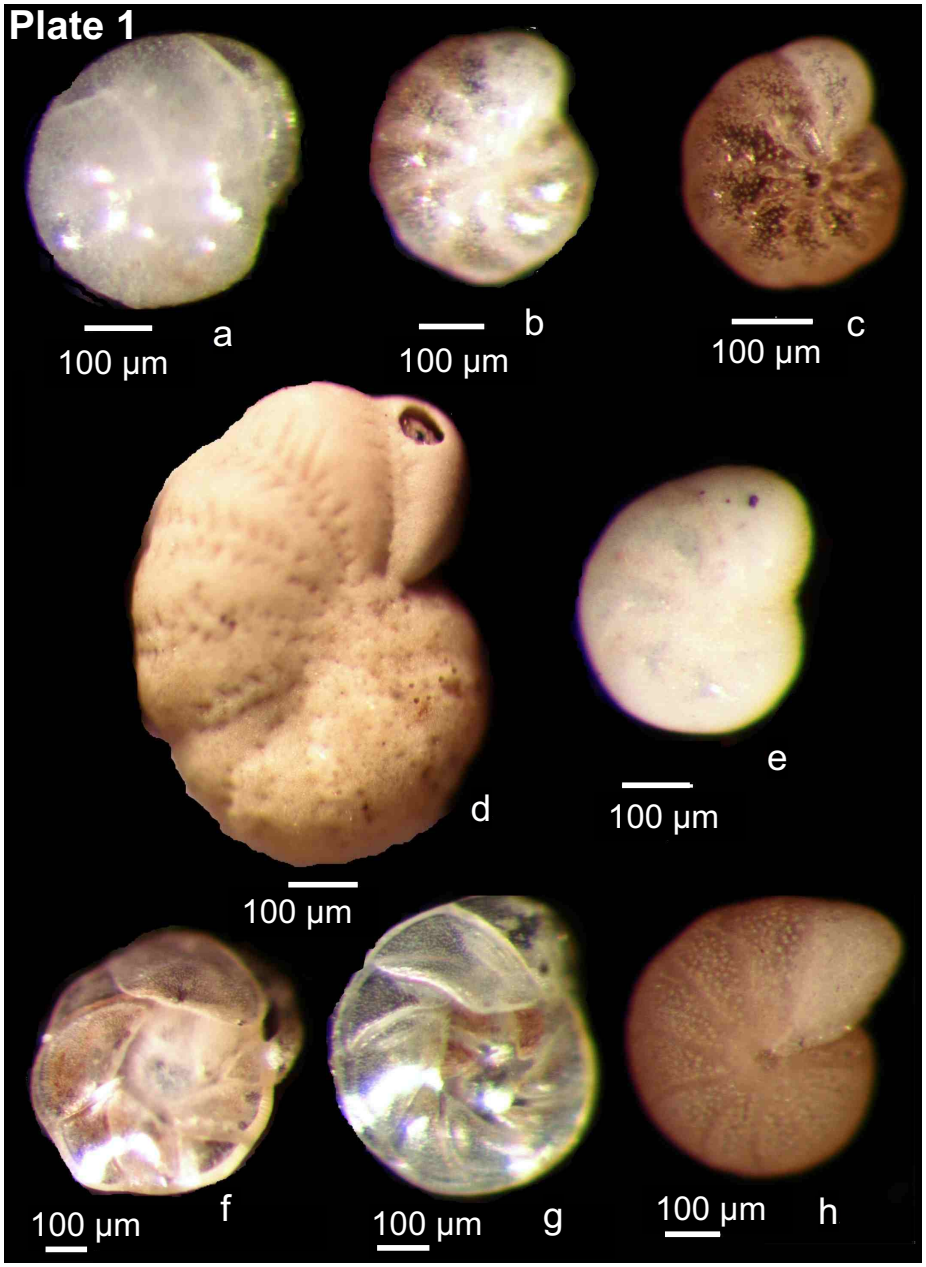
Plate 1
a
100 µm
b
100 µm
c
100 µm
d
100 µm
e
100 µm
f
100 µm
g
100 µm
h
100 µm

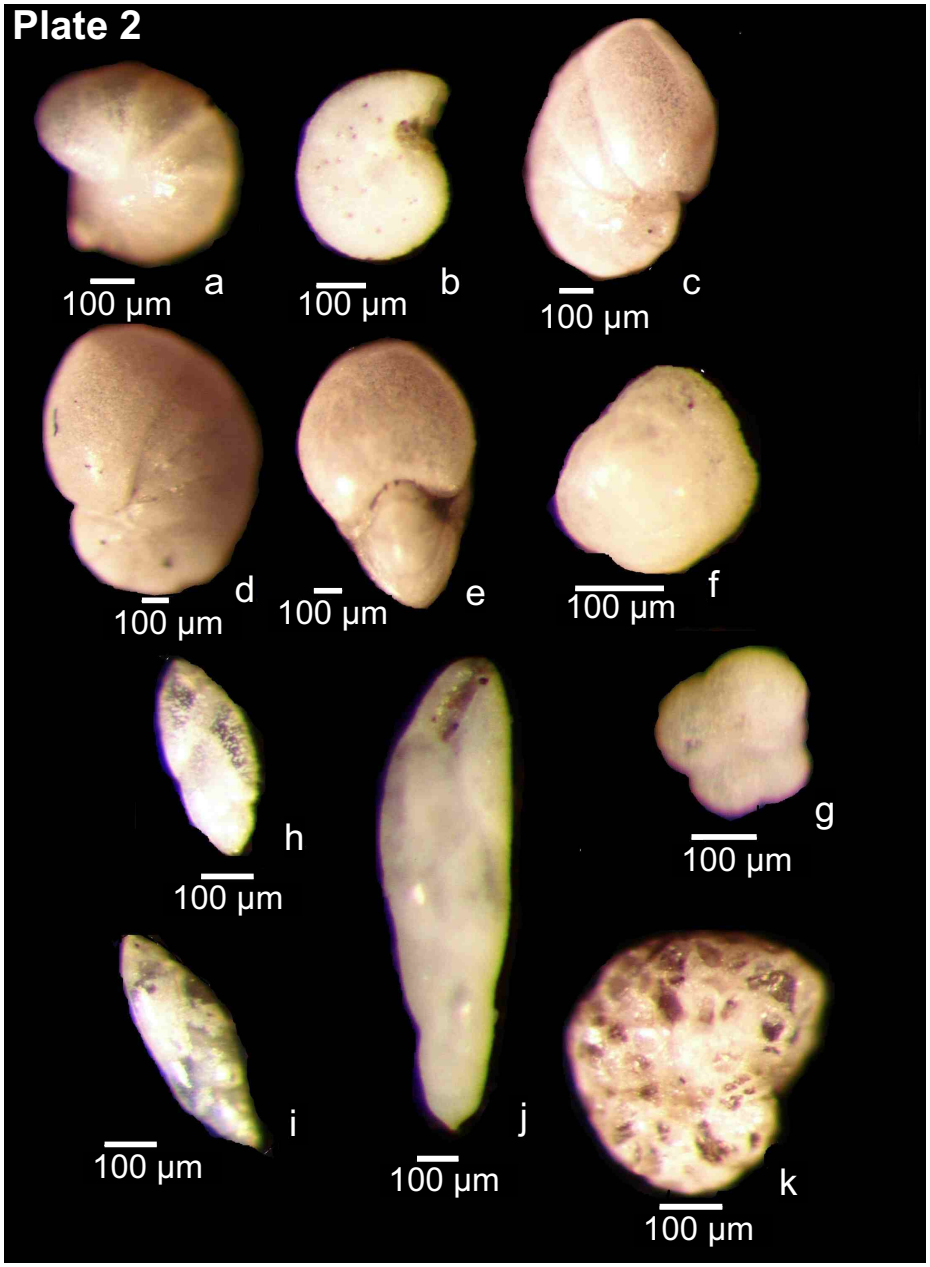
Plate 2
a
100 µm
b
100 µm
c
100 µm
d
100 µm
e
100 µm
f
100 µm
g
100 µm
h
100 µm
i
100 µm
j
100 µm
k
100 µm

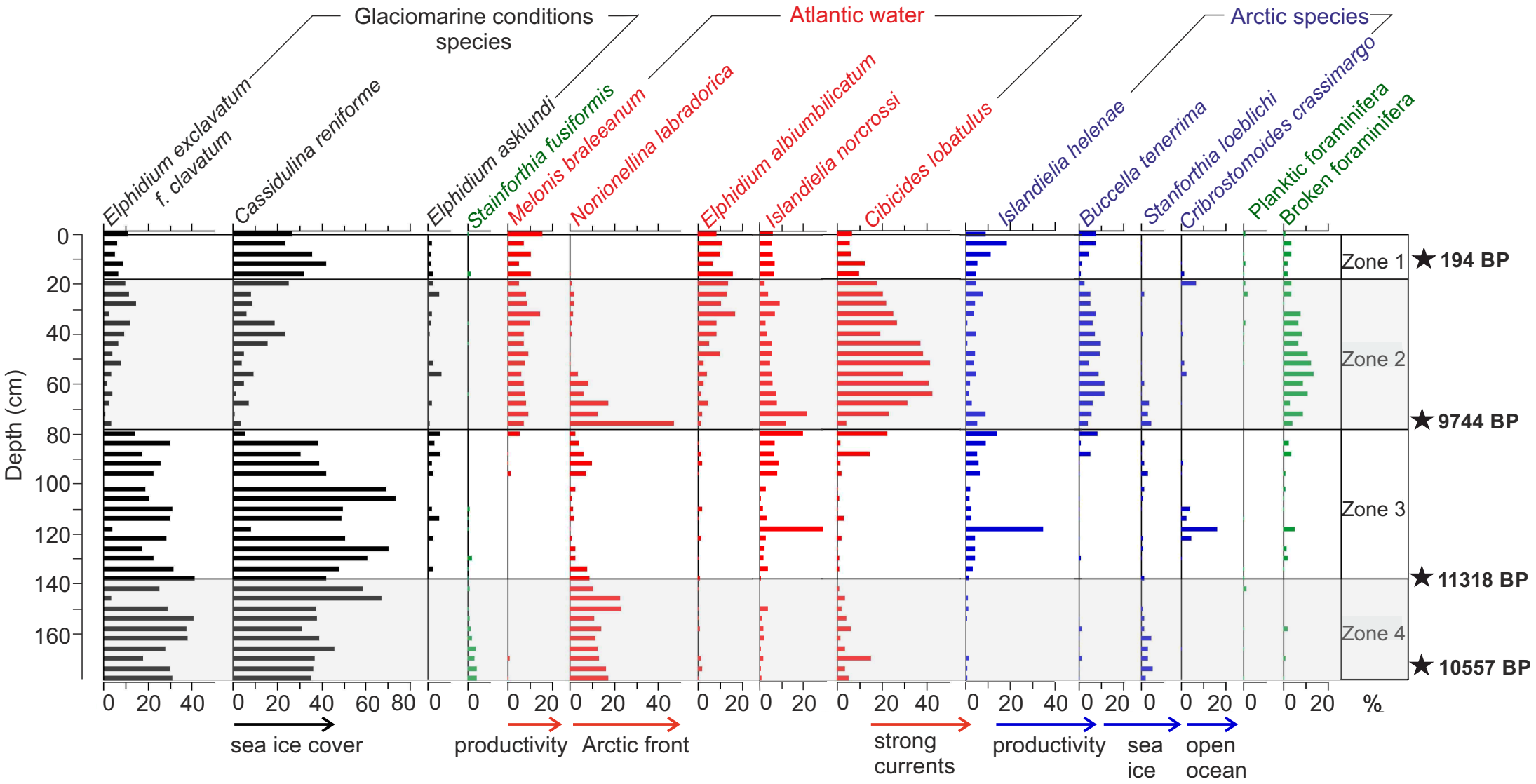
Glaciomarine conditions species
Atlantic water
Arctic species
Elphidium exclavatum f. clavatum
Cassidulina reniforme
Elphidium asklundi
Stainforthia fusiformis
Melonis braleeanum
Nonionellina labradorica
Elphidium albiumbilicatum
Islandielia norcrossi
Cibicides lobatulus
Islandielia helenae
Buccella tenerrima
Stanforthia loeblichi
Cribrostomoides crassimargo
Planktic foraminifera
Broken foraminifera
Depth (cm)
0
20
40
60
80
100
120
140
160
Zone 1
Zone 2
Zone 3
Zone 4
194 BP
9744 BP
11318 BP
10557 BP
0 20 40
0 20 40 60 80
0
0 20
0 20 40
0 20
0 20
0 20 40
0 20 40
0 20
0 20
0
0 20
%
sea ice cover
productivity
Arctic front
strong currents
productivity
sea ice
open ocean

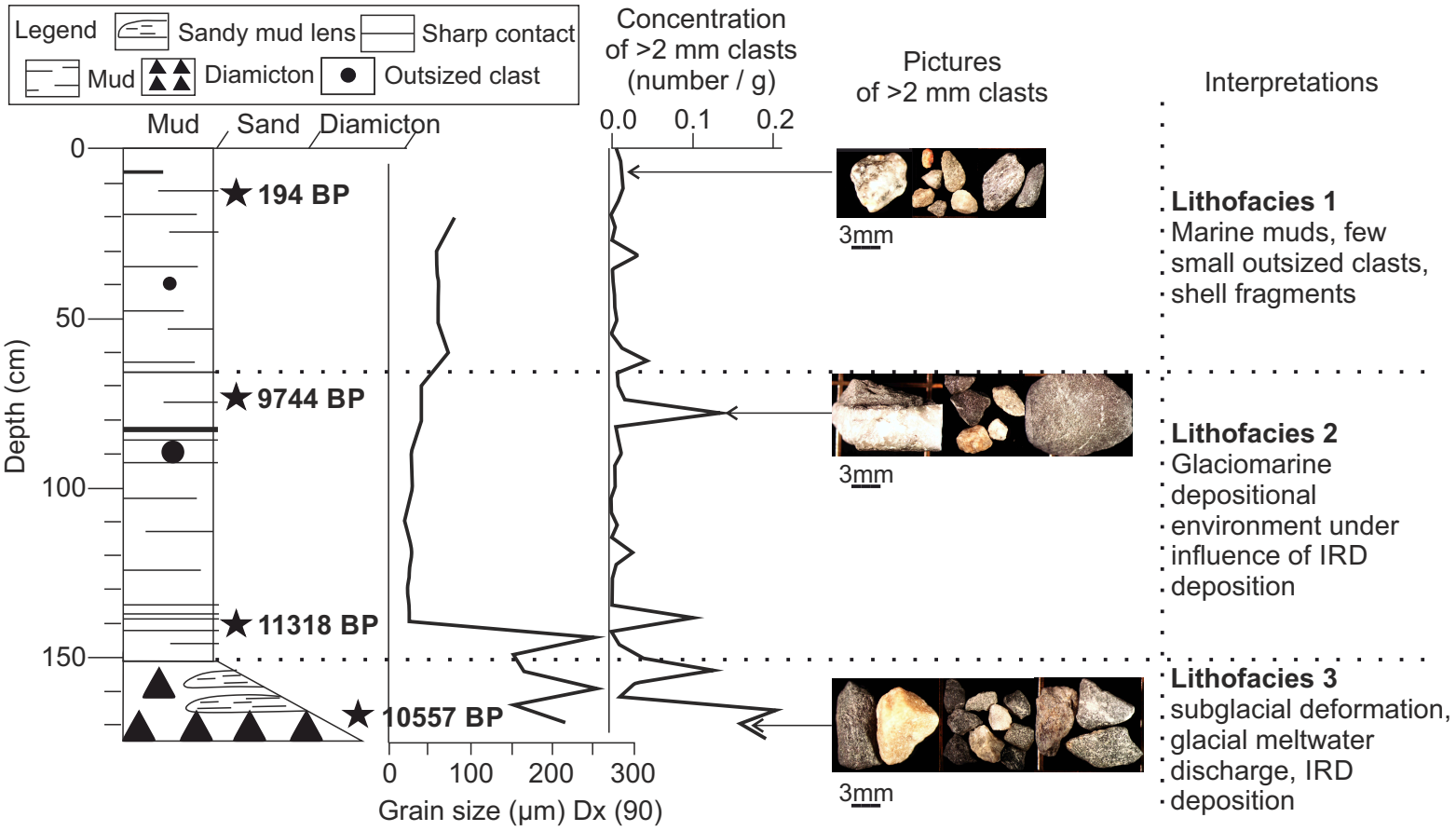
Legend
Sandy mud lens
Sharp contact
Mud
Diamicton
Outsized clast
Concentration of >2 mm clasts (number / g)
0.0
0.1
0.2
Pictures of >2 mm clasts
Interpretations
Mud
Sand
Diamicton
0
50
100
150
Depth (cm)
194 BP
9744 BP
11318 BP
10557 BP
3mm
3mm
3mm
Lithofacies 1
Marine muds, few small outsized clasts, shell fragments
Lithofacies 2
Glaciomarine depositional environment under influence of IRD deposition
Lithofacies 3
subglacial deformation, glacial meltwater discharge, IRD deposition
0
100
200
300
Grain size (µm) Dx (90)

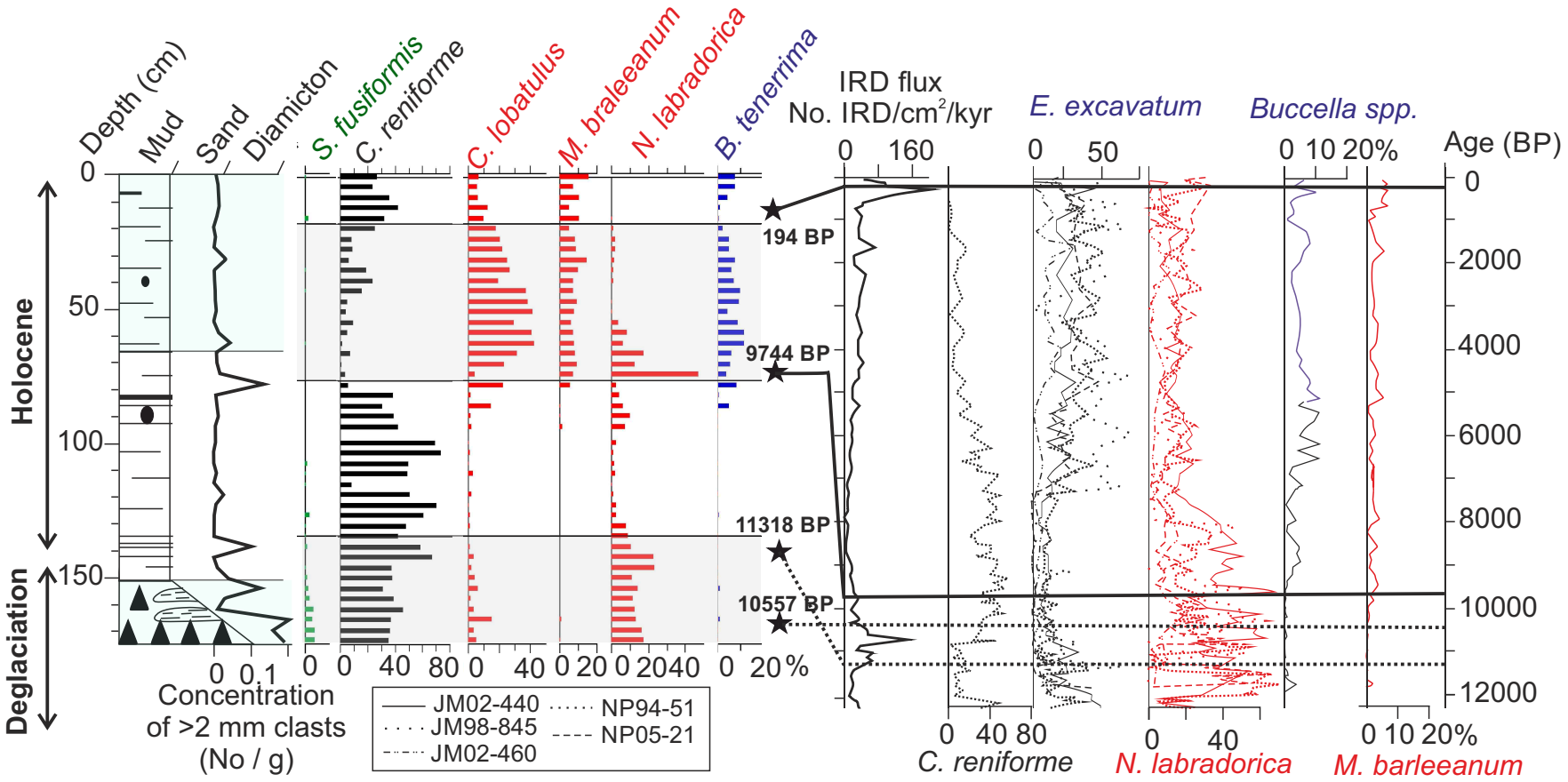
Depth (cm)
Mud
Sand
Diamicton
S. fusiformis
C. reniforme
C. lobatulus
M. braleeanum
N. labradorica
B. tenerrima
IRD flux
No. IRD/cm²/kyr
E. excavatum
Buccella spp.
Age (BP)
Holocene
Deglaciation
194 BP
9744 BP
11318 BP
10557 BP
Concentration
of >2 mm clasts
(No / g)
JM02-440
JM98-845
JM02-460
NP94-51
NP05-21
C. reniforme
N. labradorica
M. barleeanum

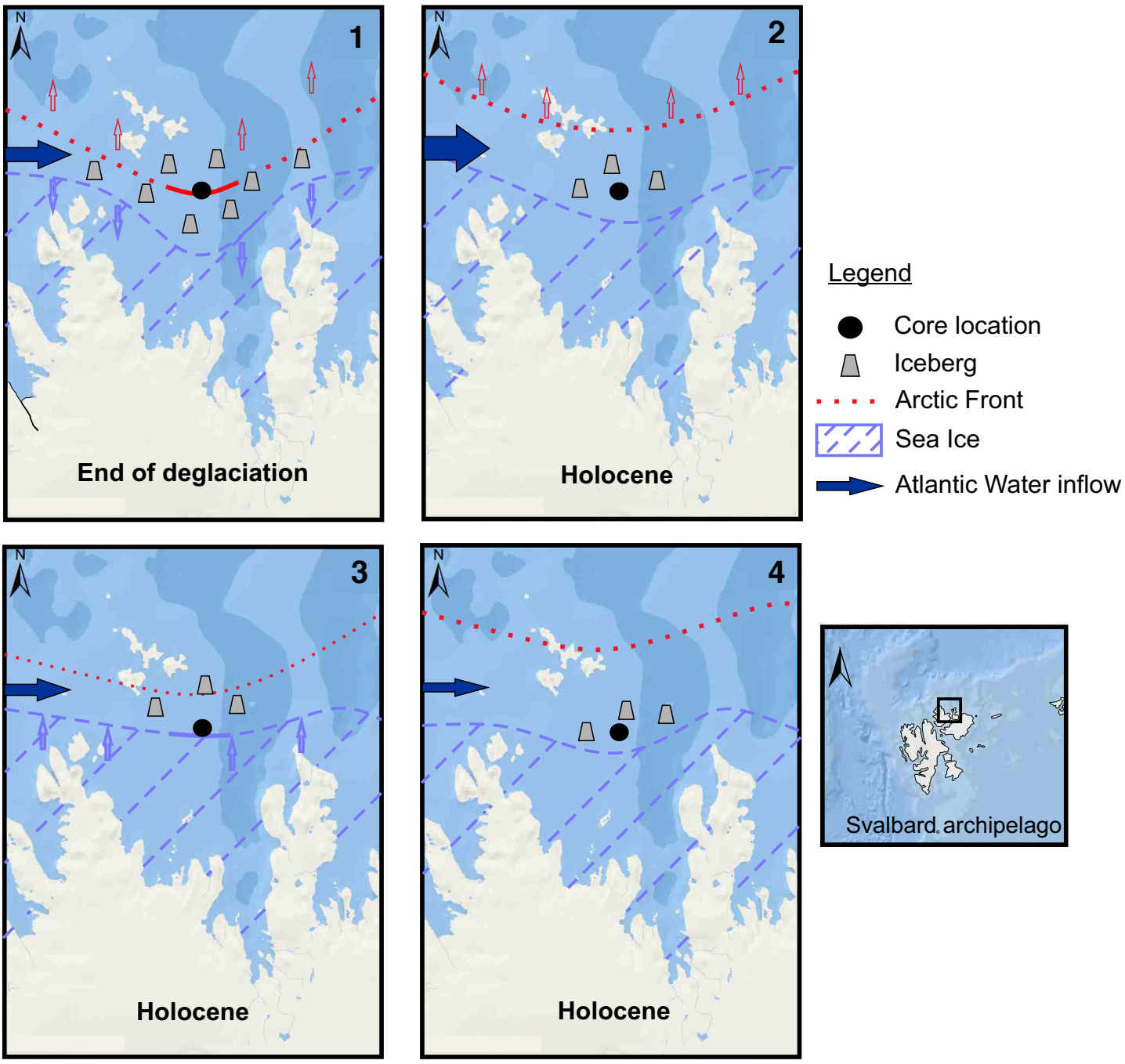
N
1
End of deglaciation
N
2
Holocene
Legend
Core location
Iceberg
Arctic Front
Sea Ice
Atlantic Water inflow
N
3
Holocene
N
4
Holocene
Svalbard archipelago